Bioactive Materials 22 (2023) 535–550

Contents lists available at ScienceDirect

Bioactive Materials

journal homepage: www.keaipublishing.com/en/journals/bioactive-materials

Fucoidan and topography modification improved *in situ* endothelialization on acellular synthetic vascular grafts

Yuan Yao [a], Aung Moe Zaw [a], Deirdre E.J. Anderson [b], YeJin Jeong [a], Joshua Kunihiro [a], Monica T. Hinds [b], Evelyn K.F. Yim [a,c,d,*]

[a] Department of Chemical Engineering, University of Waterloo, 200 University Avenue West, Waterloo, ON, N2L 3G1, Canada
[b] Department of Biomedical Engineering, Oregon Health & Science University, Portland, OR, 97239, USA
[c] Waterloo Institute for Nanotechnology, University of Waterloo, 200 University Avenue West, Waterloo, ON, N2L 3G1, Canada
[d] Center for Biotechnology and Bioengineering, University of Waterloo, 200 University Avenue West, Waterloo, ON, N2L 3G1, Canada

ARTICLE INFO

Keywords:
Blood-contacting devices
Small diameter vascular graft
Endothelialization
Topography
Fucoidan

ABSTRACT

Thrombogenesis remains the primary failure of synthetic vascular grafts. Endothelial coverage is crucial to provide an antithrombogenic surface. However, most synthetic materials do not support cell adhesion, and transanastomotic endothelial migration is limited. Here, a surface modification strategy using fucoidan and topography was developed to enable fast *in situ* endothelialization of polyvinyl alcohol, which is not endothelial cell-adhesive. Among three different immobilization approaches compared, conjugation of aminated-fucoidan promoted endothelial monolayer formation while minimizing thrombogenicity in both *in vitro* platelet rich plasma testing and *ex vivo* non-human primate shunt assay. Screening of six topographical patterns showed that 2 μm gratings increased endothelial cell migration without inducing inflammation responses of endothelial cells. Mechanistic studies demonstrated that fucoidan could attract fibronectin, enabling integrin binding and focal adhesion formation and activating focal adhesion kinase (FAK) signaling, and 2 μm gratings further enhanced FAK-mediated cell migration. In a clinically relevant rabbit carotid artery end-to-side anastomosis model, 60% *in situ* endothelialization was observed throughout the entire lumen of 1.7 mm inner diameter modified grafts, compared to 0% of unmodified graft, and the four-week graft patency also increased. This work presents a promising strategy to stimulate *in situ* endothelialization on synthetic materials for improving long-term performance.

1. Introduction

Cardiovascular diseases remain the leading cause of death globally. Synthetic vascular grafts are among crucial components in vascular reconstruction surgeries, but they have demonstrated low patency rates when replacing small diameter vessels (<6 mm). Lack of functional endothelial cell (EC) lining on the luminal surfaces has been identified as one of the primary contributors [1]. Tissue-engineered grafts that are endothelialized *in vitro* have shown promising results in animal studies [2]. However, these grafts are not off-the-shelf available due to the extended *in vitro* culture, and impaired cell function remains one of the major concerns [3]. Acellular grafts that favors *in situ* endothelialization are more appealing options. Transanastomotic migration is one of the main mechanisms of *in situ* endothelialization of acellular grafts. Bioactive molecules, such as extracellular matrix (ECM) proteins and growth factors, have been introduced to the surfaces of acellular grafts to improve EC adhesion [4]. However, studies showed these bioactive molecules present the risk of increased thrombogenicity due to the absence of specificity for ECs. Additionally, human transanastomotic endothelial migration has been shown to be limited to be 1–2 cm [5], and thus endothelialization of acellular synthetic vascular grafts was found to be mainly around the anastomosis regions while the middle of the grafts lack endothelium [6]. Thus, we sought to develop a strategy that could improve *in situ* endothelialization of acellular vascular grafts without compromising the material hemocompatibility.

Anticoagulant drug, especially heparin, has the potential to reduce

Abbreviations: PVA, Polyvinyl alcohol; STMP, Sodium trimetaphosphate; PVA-CDI-aF, Aminated fucoidan modified polyvinyl alcohol hydrogel.

Peer review under responsibility of KeAi Communications Co., Ltd.

* Corresponding author. Department of Chemical Engineering, University of Waterloo, 200 University Avenue West, Waterloo, ON, N2L 3G1, Canada.
E-mail address: eyim@uwaterloo.ca (E.K.F. Yim).

https://doi.org/10.1016/j.bioactmat.2022.10.011
Received 7 August 2022; Received in revised form 20 September 2022; Accepted 9 October 2022

thrombosis; however, it also presents a risk of hemorrhagic complications [7]. Fucoidan is a sulfated polysaccharide with similar structure as heparin. Versatile bioactivities of fucoidan have been reported [8]. Injection of fucoidan can alleviate atherosclerotic lesions by reducing leukocyte and platelet adhesion on damaged endothelium [9], inhibiting thrombin generation [10], suppressing smooth muscle cell proliferation [11], and inactivating free-radical processes [12], thus demonstrating the potential of fucoidan in cardiovascular applications [8]. Fucoidan can also mediate EC proliferation and adhesion [13], which demonstrating the potential of fucoidan as a biochemical modification molecule to improve EC adhesion without increasing thrombogenicity. However, the mechanism on how surface immobilized fucoidan could mediate cell adhesion and proliferation has not been studied.

Basement membrane presents intrinsic topography. Emerging technologies have enabled the fabrication of topography with different geometry and dimensions on synthetic materials to mimic the native environment [14]. Topography on synthetic materials has shown potential to increase cell adhesion [15]. Additionally, topography has been documented to provide contact guidance, accelerating cell migration, especially on groove structure or on aligned fibers [16]. However, previous studies showed that cell adhesion on non-adhesive materials is low, thus restricting the modulation effects of substrate topography on cell behaviors [15a,17]. Biochemical modifications that support cell adhesion while preserving the fidelity of topography will be necessary to improve the sensibility of cells to topographical cues. Moreover, topography has also been shown to direct platelet cell adhesion and activation [18]. Thus, systematically examination of the synergistic effect of biochemical cues and topography on both endothelialization and hemocompatibility is crucial.

Herein, we hypothesize that fucoidan and topography could synergistically encourage endothelialization and maintain good

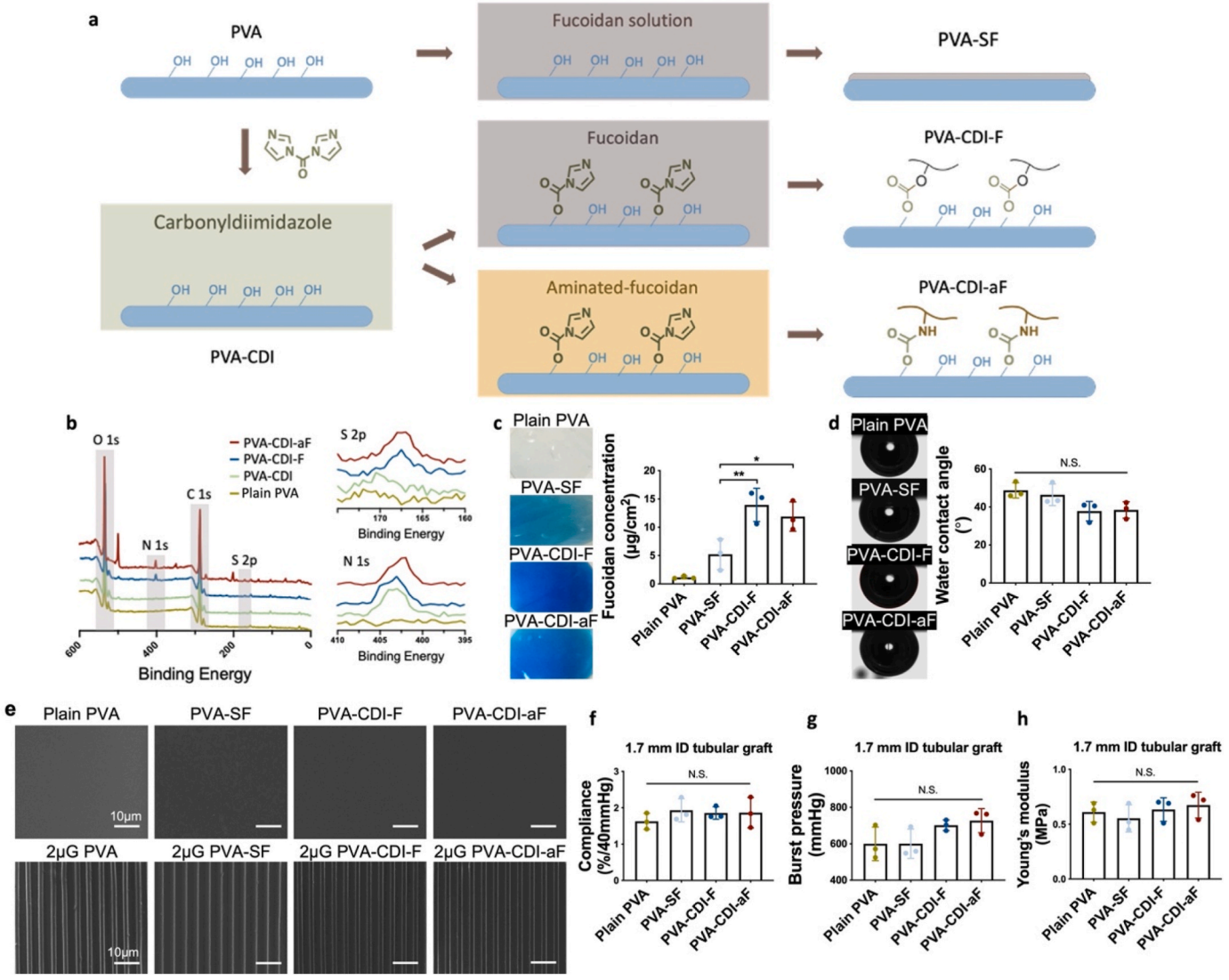

Fig. 1. Fabrication and characterization of fucoidan-modified polyvinyl alcohol (PVA) hydrogels. (**a**) Schematic diagram of fucoidan modification procedures. PVA-SF was prepared by soaking PVA in native fucoidan solution. PVA-CDI-F was prepared by conjugating native fucoidan on PVA through carbonyldiimidazole (CDI) reaction. PVA-CDI-aF was prepared by conjugating aminated-fucoidan (aF) on PVA through CDI reaction. (**b**) X-ray photoelectron spectroscopy (XPS) survey scan of plain PVA, CDI-activated PVA (PVA-CDI), PVA-CDI-F, and PVA-CDI-aF. (**c**) Quantification of fucoidan concentration by toluidine blue staining. n = 3, * and ** indicate a significant difference using one-way ANOVA with $p < 0.05$ and $p < 0.01$, respectively. (**d**) Water contact angle measurement using a captive bubble device. n = 3, N.S. indicates no significant difference. (**e**) Scanning electron microscope (SEM) images of unpatterned and unmodified PVA (plain PVA), unpatterned PVA-SF, unpatterned PVA-CDI-F and unpatterned PVA-CDI-aF and 2 μm gratings patterned PVA (2 μG PVA), PVA-SF (2 μG PVA-SF), PVA-CDI-F (2 μG PVA-CDI-F) and PVA-CDI-aF (2 μG PVA-CDI-aF). Scale bar = 10 μm. (**f**) Compliance, (**g**) burst pressure, and (**h**) Young's modulus of PVA, PVA-SF, PVA-CDI-F and PVA-CDI-aF tubular grafts with 1.7 mm inner (ID) diameter. n = 3, N.S. indicates no significant difference.

hemocompatibility. Polyvinyl alcohol (PVA) has been widely used in various biomedical applications [19]. Our previous studies demonstrated that PVA hydrogel chemically crosslinked by sodium trimetaphosphate (STMP) is a promising vascular graft material due to tunable mechanical properties, good biocompatibility, and low platelet adhesion and thrombin generation [13d,20], However, PVA hydrogel does not support cell adhesion. In this study, we used STMP-crosslinked PVA hydrogel as a platform to deliver both fucoidan and topography to improve *in situ* endothelialization of PVA while minimizing thrombogenicity. We systematically examined the effects of different fucoidan immobilization strategies and various micro-sized topographies on EC adhesion, monolayer formation, and inflammatory responses and hemocompatibility in both *in vitro* platelet rich plasma testing and *ex vivo* non-human primate whole blood flow shunt model. Additionally, the underlying mechanisms of fucoidan- and topography-mediated EC responses were explored. By inhibiting phosphorylation of focal adhesion kinase (FAK), we demonstrated that fucoidan facilitated cell adhesion and topography improved cell migration via focal adhesion (FA) signaling. Furthermore, we assessed the efficiency of fucoidan immobilization and topographical modification in improving *in situ* endothelization and graft patency in a clinically relevant end-to-side rabbit carotid artery implantation model.

2. Results

2.1. Fabrication and characterization of fucoidan-modified PVA hydrogels

PVA hydrogels were fabricated by chemical crosslinking using STMP, as previously reported [20b]. The PVA hydrogels were subsequently modified with fucoidan by soaking method or conjugation reactions, as shown in Fig. 1a. PVA-SF was prepared by soaking PVA in native fucoidan solution. Fucoidan conjugation on PVA was performed via carbonyldiimidazole (CDI) reaction [21]. CDI-activated PVA (PVA-CDI) was prepared as a control. PVA-CDI-F was prepared by conjugating native fucoidan on PVA-CDI. In order to facilitate fucoidan conjugation on PVA-CDI, we synthesized aminated-fucoidan (aF) by reacting native fucoidan with ethylenediamine (EDA) via CDI reaction. The structure of aF was confirmed by the characteristic peaks in 1H NMR spectra (Supplementary Fig. 1). PVA-CDI-aF was then prepared by conjugating aF on PVA-CDI. X-ray photoelectron spectroscopy (XPS) demonstrated the presence of N1s peaks on PVA-CDI, PVA-CDI-F and PVA-CDI-aF and S2p peaks on PVA-CDI-F and PVA-CDI-aF (Fig. 1b), revealing the success of fucoidan conjugation on PVA.

To examine the effect of amination condition on the activities of aF, a series of aF molecules with increasing EDA to fucoidan molar ratio (aF [EDA/fucodan ratio]: aF2, aF5, aF10, and aF25) were prepared (Supplementary Figs. 2a and b). PVA-CDI-aF prepared using the different aF molecules did not show significantly difference in the surface energy compared to unmodified PVA (Supplementary Fig. 2c). PVA-CDI-aF25 demonstrated the highest fucoidan concentration and cell adhesion, and the lowest thrombogenicity (Supplementary Figs. 2d,3,4), and thus PVA-CDI-aF25 was used for the rest of the work.

To determine the most efficient modification method to immobilize fucoidan on PVA, the surface properties of PVA-SF, PVA-CDI-F, and PVA-CDI-aF were characterized. Toluidine blue staining verified the presence of fucoidan on modified PVA and showed that PVA-CDI-F and PVA-CDI-aF had higher fucoidan concentration than PVA-SF (Fig. 1c). After fucoidan-modification, the water contact angle (WCA) decreased slightly but not significantly (Fig. 1d). In order to assess if the fucoidan modifications are compatible with surface patterning, we prepared unpatterned and 2 μm grating (2 μG) patterned PVA films and modified with fucoidan. Scanning electron microscope (SEM) images showed that the surface roughness of unpatterned samples and the fidelity of the 2 μG pattern were not affected by any of the fucoidan-modifications (Fig. 1e). Furthermore, we assessed the effect of the different fucoidan modifications on the mechanical properties of PVA small diameter vascular grafts. 1.7 mm inner diameter (ID) PVA, PVA-SF, PVA-CDI-F, and PVA-CDI-aF tubular grafts were fabricated. The compliance, burst pressure, and Young's modulus did not show significant difference among the four groups, demonstrating that the fucoidan modifications did not alter the mechanical properties of PVA grafts. (Fig. 1f–h).

2.2. Aminated-fucoidan promotes endothelial cell adhesion without increasing thrombogenicity

To evaluation the effects of fucoidan-modification on EC adhesion on PVA, we assessed the human umbilical vein endothelial cell (HUVEC) adhesion and monolayer formation on both plain PVA (unmodified and unpatterned) and fucoidan-modified PVA films. Only a few cells attached to plain PVA, while after fucoidan modification, cell adhesion was substantially promoted ($n = 6$, $p < 0.0001$), and the cells were able to form monolayers, with strong expression of platelet endothelial cell adhesion molecule-1 (PECAM-1 or CD31) and VE-cadherin at the cell boundaries (Fig. 2a,c-e). Comparing the three fucoidan-modified PVA groups, PVA-CDI-F and PVA-CDI-aF had higher CD31 expression than PVA-SF (Fig. 2d), suggesting the formation of more mature EC monolayers. Additionally, HUVECs on PVA-SF, PVA-CDI-F, and PVA-CDI-aF, when being seeded at a lower density, demonstrated significantly larger cell area and FA size compared to those on plain PVA (Fig. 2b,f).

We next comprehensively examined the hemocompatibility of fucoidan-modified PVA *in vitro* using rabbit platelet rich plasma and *ex vivo* using a non-human primate whole blood flow shunt study. *In vitro* testing was done with film samples. SEM images showed that platelets on the positive control, collagen-coated glass, exhibited activated morphology (Fig. 2g). Clinical control, expanded polytetrafluoroethylene (ePTFE), plain PVA, and PVA-CDI-aF demonstrated significantly lower platelet adhesion compared to collagen coated glass ($p < 0.01$), and the adhered platelets exhibited non-activated morphology (Fig. 2g and h). Similarly, ePTFE, plain PVA, and PVA-CDI-aF had decreased thrombin generation compared to collagen-coated glass ($n = 5$, $p < 0.001$) (Fig. 2i and j and Supplementary Fig. 5a). Comparing the three fucoidan modifications, PVA-CDI-aF reduced platelet adhesion and suppressed peak ($n = 5$, $p < 0.0001$) and total thrombin generation ($p < 0.01$) compared to PVA-SF and PVA-CDI-F. *Ex vivo* shunt studies using non-human primate was performed on 4 mm inner diameter (ID) tubular grafts. After the 1-h whole blood flow, PVA-CDI-aF tubular grafts had significantly lower platelet accumulation ($n = 6$, $p < 0.001$) and decreased fibrin accumulation ($n = 6$, $p < 0.01$) compared to PVA-SF and PVA-CDI-F grafts (Fig. 2k,l). A higher patent luminal area was also observed in PVA-CDI-aF grafts, compared to PVA-SF and PVA-CDI-F grafts (Supplementary Fig. 5b). These results showed that only PVA-CDI-aF promoted endothelialization without compromising the hemocompatibility of PVA.

2.3. Synergistic effect of aminated-fucoidan and topography

To further improve EC responses, we fabricated PVA-CDI-aF hydrogels with various topographies, including 2 μm gratings (2 μG), 5 μm gratings (5 μG), 10 μm gratings (10 μG), 2 μm pillars (2 μP), 1.8 μm concave lenses (CCV), and 1.8 μm convex lenses (CVX). SEM images demonstrated good shape fidelity of all topographies on PVA-CDI-aF (Supplementary Fig. 6a and Supplementary Table 2). Patterned PVA-CDI-aF did not show a significant difference in WCA compared to plain PVA (unmodified and unpatterned) and unpatterned (UP) PVA-CDI-aF (Supplementary Figs. 6b and c). HUVECs exhibited good attachment on all PVA-CDI-aF samples and formed confluent monolayers with strong VE-cadherin expression at the cell boundaries (Fig. 3a). The different topographies on PVA-CDI-aF did not significantly alter the cell density, area, nor VE-cadherin expression level (Fig. 3b–d). Importantly, the grating structures decreased cell circularity ($n = 6$, $p < 0.01$) and induced cell elongation along the grating axis (Fig. 3a,e).

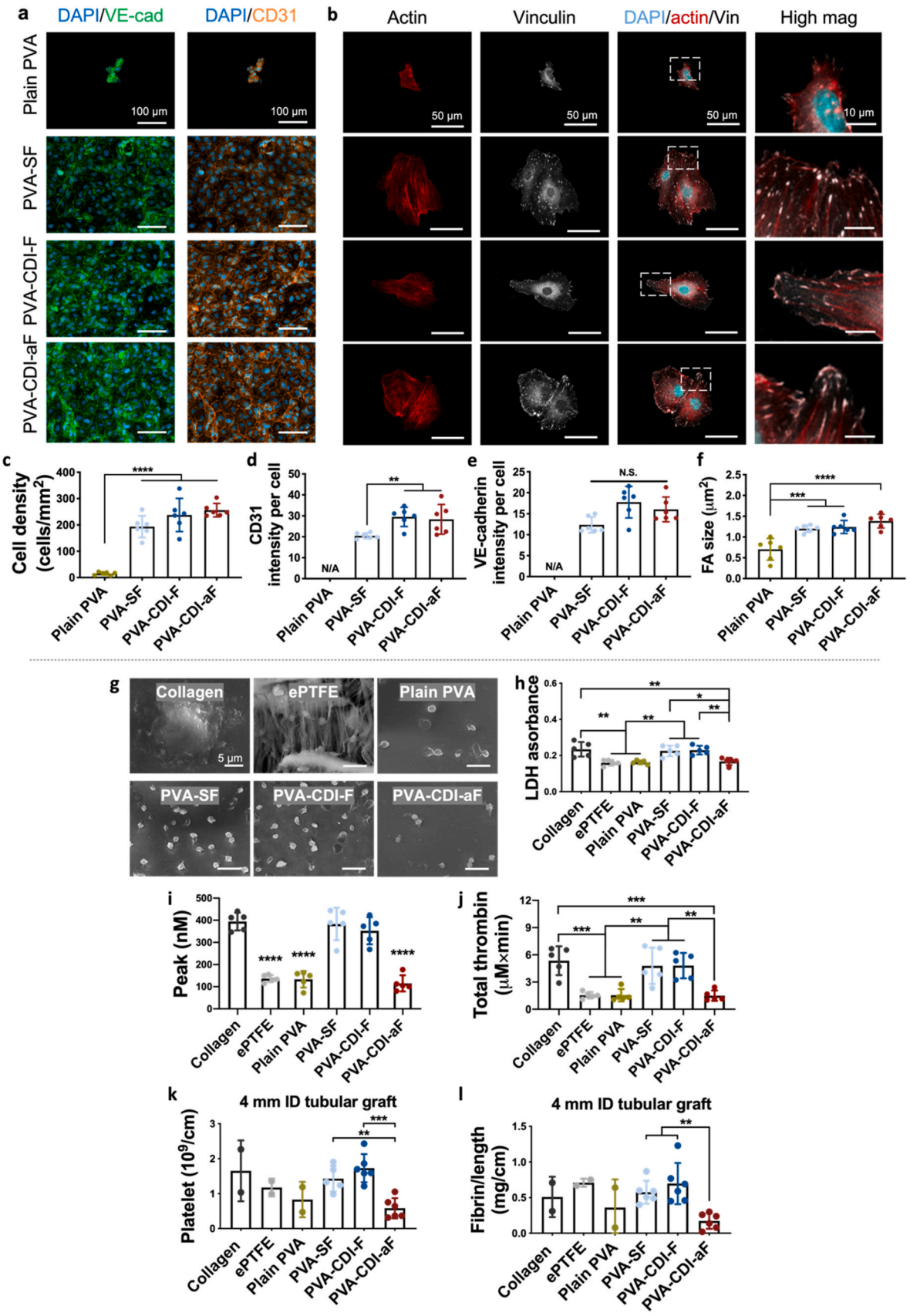

(caption on next page)

Fig. 2. Endothelialization and hemocompatibility of fucoidan-modified PVA hydrogels. (**a**) Immunofluorescence staining images of VE-cadherin (green) and platelet endothelial cell adhesion molecule-1 (PECAM-1/CD31, orange) expression by human umbilical vein endothelial cells (HUVECs) on plain PVA and fucoidan-modified PVA. Scale bar = 100 μm. (**b**) Immunofluorescence staining images of F-actin (red) and focal adhesion (FA) formation (vinculin, grey) by HUVECs on plain PVA and fucoidan-modified PVA. Scale bar = 50 μm. Quantification of (**c**) cell density, (**d**) VE-cadherin and (**e**)CD31 expression, and (**f**) FA size. N/A indicates not applicable. Plain PVA was not included in the VE-cadherin and CD31 comparison due to the low number of adhered cells. n = 6, **, ***, and **** indicate a significant difference using one-way ANOVA with $p < 0.01$, $p < 0.001$, and $p < 0.0001$, respectively. (**g**) Representative SEM images of platelets on plain PVA and fucoidan-modified PVA. Collagen-coated glass and expanded polytetrafluoroethylene (ePTFE) were included as controls. Scale bar = 5 μm. (**h**) Quantification of platelet adhesion determined by lactate dehydrogenase (LDH) assay. (i,**j**) Realtime thrombin generation using rabbit platelet rich plasma: (**i**) Peak represents the maximum thrombin generation rate. (**j**) Total thrombin represents the total amount of thrombin generated during the test period. n = 5, *, **, ***, and **** indicate a significant difference using one-way ANOVA with $p < 0.05$, $p < 0.01$, $p<0.001$, and $p < 0.0001$, respectively. (k,**l**) Ex vivo shunt assay using non-human primate model: (**k**) Platelet accumulation and (**l**) fibrin accumulation after 1 h of whole blood flow. Collagen–coated ePTFE (n = 2), ePTFE (n = 2), and plain PVA (n = 2) tubular grafts with 4 mm inner diameter were not included in the statistical analysis due to the low number of tested samples. n = 6 for PVA-SF, PVA-CDI-F, and PVA-CDI-aF tubular grafts with 4 mm inner diameter. **, and *** indicate a significant difference using one-way ANOVA with $p < 0.01$ and $p < 0.001$, respectively.

A low level of monocyte adhesion on ECs and low expression of pro-inflammatory markers are indicators of an anti-inflammatory surface [22]. To evaluate the effect of substrate topography on endothelial cell interaction with monocytes, endothelial cells were cultured on unpatterned and patterned PVA-CDI-aF until confluency, and monocyte adhesion on endothelium was activated by (tumor necrosis factor α) TNF-α. Plain PVA was not included in the study due to the lack of endothelial monolayer formation. Unpatterned (UP) and 2 μm gratings (2 μG) PVA-CDI-aF demonstrated the lowest monocyte adhesion on endothelial monolayers among all patterns (Fig. 3f and g). 10 μm gratings (10 μG) and 2 μm pillars (2 μP) PVA-CDI-aF induced a significantly higher monocyte adhesion, compared to UP and 2 μG PVA-CDI-aF (n = 6, $p < 0.05$). The CD31 expression remained unchanged across the topographies (Fig. 3h), while intercellular adhesion molecule 1 (ICAM-1) expression was significantly elevated by cells on 2 μP PVA-CDI-aF compared to those on UP and 2 μG PVA-CDI-aF (n = 6, $p < 0.01$) (Fig. 3i).

Comparing the hemocompatibility of PVA-CDI-aF with different topographies, plain PVA and all PVA-CDI-aF samples had lower platelet attachment and thrombin generation compared to collagen in the *in vitro* test with platelet-rich plasma (PRP) (Fig. 3j-l and Supplementary Figs. 6a and b). The adhered platelets on plain PVA and all PVA-CDI-aF were rounded and exhibited non-activated morphology. No significant difference was observed among the PVA-CDI-aF groups. PVA-CDI-aF tubular grafts that were unpatterned or patterned with 2 μG and 10 μG were further examined *ex vivo* using the non-human primate shunt study. The platelet accumulation after 1 h of whole blood flow in 2 μG and 10 μG PVA-CDI-aF grafts were higher compared to those in UP PVA-CDI-aF (Fig. 3m). While not compared statistically, this accumulation was at a level comparable to the plain PVA and well below the clinical ePTFE controls. No significant change was observed in fibrin accumulation nor average patent luminal area (Supplementary Figs. 7c–d and Fig. 3n).

To understand the adhesion mechanism of these surface modifications, additional studies on FA formation and cell migration were performed.

2.4. Focal adhesion kinase in fucoidan- and topography-mediated endothelial cell adhesion and migration

Cells adhere to substrates or ECM proteins via integrins and FAs. Adhered HUVECs on unpatterned PVA-CDI-aF samples exhibited positive staining of integrin subunits β_1, α_2, α_5, α_6, and integrin $\alpha_v\beta_5$ (Fig. 4a). Laminin (LMN) has been reported to provide ligands for $\alpha_2\beta_1$, $\alpha_6\beta_1$, and $\alpha_v\beta_5$ [23], and gelatin (GEL) provides ligand for integrin $\alpha_5\beta_1$ [24]. We compared the FA formation on PVA-CDI-aF, PVA-CDI-GEL and PVA-CDI-LMN (Fig. 4b) with vinculin staining. HUVECs formed comparable number of FAs, although the FA size on PVA-CDI-LMN was larger than PVA-CDI-aF (Fig. 4c and d).

Transanastomotic migration has been identified as one of the primary *in situ* endothelialization mechanisms in acellular vascular graft. HUVECs on 2 μG PVA-CDI-aF had a significantly faster wound closure speed (Fig. 4e and f) compared to those on UP PVA-CDI-aF. Furthermore, we observed larger FAs on 2 μG PVA-CDI-aF (Supplementary Fig. 8). To explore the involvement of topography-induced FA signaling in EC adhesion and migration on UP and 2 μG PVA-CDI-aF, an inhibitor of FAK autophosphorylation, Y15, was added to the cell culture. Y15 decreased the cell migration on UP and 2 μG PVA-CDI-aF samples in a dose-dependent manner (Fig. 4g). 1 μM Y15 significantly slowed down the cell migration on 2 μG PVA-CDI-aF, and the wound closure percentage at 9 h was similar to that on UP PVA-CDI-aF (Fig. 4i). Furthermore, 10 μM Y15 impaired the cell adhesion on UP PVA-CDI-aF but not on 2 μG PVA-CDI-aF (Fig. 4h), suggesting that 2 μm grating increased FAK activities. Overall, the results demonstrated the involvement of FAK signaling in fucoidan- and 2 μG-promoted EC adhesion and migration.

2.5. Role of ECM and fucoidan in endothelial cell adhesion and migration

To further explore how fucoidan facilitates cell adhesion, cell adhesion and migration in both serum containing media (EGM) and serum free media (SFM) were compared. HUVECs attached to PVA-CDI-aF in both EGM and SFM; however, cell density, area, FA size and cell migration were significantly decreased in SFM (Fig. 5 a-f). Conversely, after adding fibronectin in SFM (SFM/fn), cell adhesion was recovered (Fig. 5a–d), and the cell migration on both UP and 2 μG PVA-CDI-aF was also significantly enhanced (Fig. 5e and f). Moreover, the cell migration on PVA-CDI-aF in SFM/fn also involves FAK signaling, similar to that in EGM (Supplementary Fig. 9). The results demonstrated the crucial role of fibronectin in PVA-CDI-aF-mediated EC adhesion.

We next investigated HUVEC adhesion on fibronectin-coated PVA-CDI-aF in SFM. HUVECs on fibronectin-coated PVA-CDI-aF were more spread and had larger FA formation, visualized with vinculin and phosphorylated FAK (pFAK) staining, compared to non-coated PVA-CDI-aF (Fig. 5g,i-k). To evaluate the EC monolayer formation, cells were cultured on PVA-CDI-aF in SFM for 3 days. After 3 days, cell densities on 1–10 μg/cm^2 fibronectin-coated PVA-CDI-aF were significantly higher and cells on PVA-CDI-aF coated with 5 and 10 μg/cm^2 fibronectin were able to express VE-cadherin at the cell boundaries (Fig. 5h,l). Conversely, plain PVA and PVA-CDI had low cell adhesion even with 5 μg/cm^2 fibronectin coating. (Supplementary Fig. 10). The results suggested that fucoidan could present fibronectin to ECs to improve cell adhesion.

2.6. Fucoidan and 2uG improved endothelialization in vivo

To determine the proper sterilization method for *in vivo* studies, we compared EC adhesion and thrombin generation of gamma irradiated (GM) and ethylene oxide (EtO) sterilized PVA-CDI-aF. Neither of the sterilizations changed HUVEC adhesion (Supplementary Figs. 11a and b), while only EtO maintained the low thrombogenicity (Supplementary Figs. 11c–e), thus EtO was chosen as the terminal sterilization method for implanted grafts.

The *in vivo* endothelialization and patency of plain PVA, UP PVA-CDI-aF, and 2 μG PVA-CDI-aF tubular grafts with 1.7 mm inner

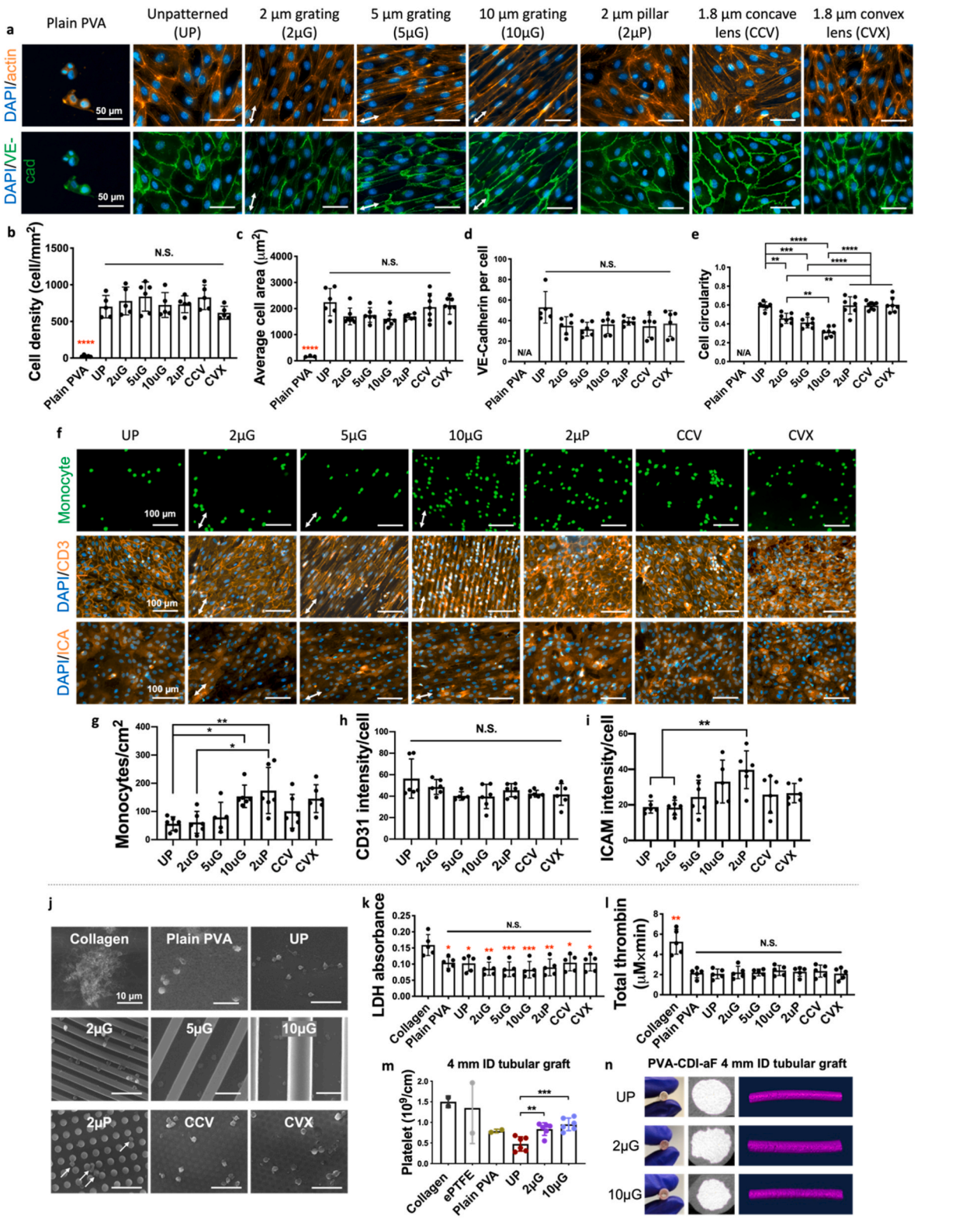

(caption on next page)

Fig. 3. Endothelialization and hemocompatibility of unpatterned and patterned PVA-CDI-aF. (**a**) Immunofluorescence staining images of VE-cadherin and actin staining of endothelial cells on unpatterned and unmodified PVA (plain PVA), unpatterned PVA-CDI-aF (UP), 2 μm grating PVA-CDI-aF (2 μG), 5 μm grating PVA-CDI-aF (5 μG), 10 μm grating PVA-CDI-aF (10 μG), 2 μm grating PVA-CDI-aF (2 μP), 1.8 μm concave lens PVA-CDI-aF (CCV), and 1.8 μm convex lens PVA-CDI-aF (CVX). Scale bar = 50 μm. Arrows indicate the directions of gratings. Quantification of (**b**) cell density, (**c**) average cell area, (**d**) VE-cadherin expression, and (**e**) cell circularity. n = 6, black **, ***, and **** indicate a significant difference using one-way ANOVA with $p < 0.01$, $p < 0.001$, and $p < 0.0001$, respectively, among PVA-CDI-aF samples. Red **** indicates a significant difference using one-way ANOVA with $p < 0.0001$ compared to plain PVA. N/A indicated not applicable. (**f**) Immunofluorescence staining images of monocyte adhesion and staining of CD31 and intercellular Adhesion Molecule 1 (ICAM-1) of HUVECs on unpatterned and patterned PVA-CDI-aF. Monocyte adhesion on endothelium was activated by tumor necrosis factor α (TNF-α). Plain PVA was not included due to the lack of confluent endothelial monolayer formation. Scale bar = 50 μm. Arrows indicate the directions of gratings. Quantification of (**g**) monocyte density, (**h**) CD31 expression, and (**i**) intercellular adhesion molecule 1 (ICAM-1) expression. n = 6, * and ** indicate a significant difference using one-way ANOVA with $p < 0.05$ and $p < 0.01$, respectively. N.S. indicates no significant difference. (**j**) Representative SEM images of adhered platelets on collagen-coated glass, plain PVA, and unpatterned and patterned PVA-CDI-aF. Scale bar = 10 μm. (**k**) Quantification of platelet adhesion determined by LDH assay and (**l**) Total thrombin determined from *in vitro* hemocompatibility test using rabbit platelet rich plasma. n = 5, Red *, **, and ***, indicate a significant difference using one-way ANOVA with $p < 0.05$, $p < 0.01$, and $p < 0.001$, respectively, compared to collagen group. N.S. indicates no significant difference among all PVA groups. (**m**) Platelet accumulation after 1 h of whole blood flow determined from *ex vivo* non-human primate shunt assay. Collagen–coated ePTFE (n = 2), ePTFE (n = 2), plain PVA (n = 2), and unpatterned (UP), 2 μm grating (2 μG), and 10 μm grating (10 μG) PVA-CDI-aF (n = 6) tubular grafts with 4 mm inner diameter (ID) were tested. ** and *** indicate a significant difference using one-way ANOVA with $p < 0.01$ and $p < 0.001$. Collagen-coated ePTFE, ePTFE, and plain PVA were not included in the statistical analysis. (**n**) Patent luminal areas of samples tested after 60 min of whole blood flow.

diameter, 2 cm length and curvature of 1.4 cm radius in the middle were examined in a rabbit right common carotid artery model using end-to-side anastomosis (Supplementary Fig. 12). Plain PVA, UP PVA-CDI-aF, and 2 μG PVA-CDI-aF grafts had 4-week patency rates of 75%, 75%, and 80%, respectively. The blood flow velocity in both UP and 2 μG PVA-CDI-aF grafts was 2 times higher than that in plain PVA grafts at 2 weeks and 4 weeks after implantation (Fig. 6a–c). Successful EC adhesion was observed on both UP PVA-CDI-aF and 2 μG PVA-CDI-aF grafts, while no cells attached to the surfaces of plain PVA grafts (Fig. 6d). Furthermore, we compared the endothelialization at different locations along the grafts. Endothelial coverage around the anastomoses was comparable between 2 μG PVA-CDI-aF and UP PVA-CDI-aF grafts, however, endothelial coverage at the mid-point and the percentage of grafts that are endothelialized (>50% endothelial coverage) in the mid-point of 2 μG PVA-CDI-aF grafts were twice as high as those of UP PVA-CDI-aF grafts (Fig. 6e and f). H&E staining showed significant amount of blood clot in the plain PVA, while minimal clot was seen in PVA-CDI-aF grafts (Fig. 6g). The stenosis percentage did not exhibit statistical significance (Fig. 6h). Masson's trichrome staining demonstrated no significant difference in the percentage of collagen and smooth muscle cells among all groups (Fig. 6i).

The *in vivo* studies demonstrated the efficacy of aminated-fucoidan and 2 μG topography in improving endothelialization throughout the PVA small diameter vascular graft.

3. Discussion

Endothelialization on synthetic vascular graft materials is crucial to prevent thrombosis and maintain graft patency. The primary graft endothelialization methods are transanastomotic migration of ECs from the native vasculature, capture of circulating endothelial progenitor cells, and transmural migration [5]. Previous biomaterials work has focused on the first two approaches to improve *in situ* endothelialization. Surface immobilization of ECM proteins has shown efficacy in promoting EC adhesion to graft surfaces [25]. However, the non-specific adhesion of platelets may induce thrombosis formation before EC adhesion occurs. Furthermore, migration of ECs from native artery is limited in human patients and is not sufficient to endothelialize long acellular grafts. Hence, developing a durable acellular vascular graft remains challenging. Our previous studies showed the potential of STMP-crosslinked PVA hydrogels in vascular graft application [20b,20c, 26]. Using the PVA hydrogels as a platform, we here demonstrate a strategy of combinational delivery of fucoidan and topography to enhance endothelialization without compromising hemocompatibility.

Immobilized fucoidan has been shown to increase EC adhesion [11, 13b-d]. When we previously mixed fucoidan into PVA hydrogels, a significant surface roughness change of PVA hydrogels was observed [13d]. Similarly, fucoidan immobilization on plasma treated polyethylene terephthalate surfaces changed the surface morphology [27]. Here, we selected a zero-length linker, CDI, and successfully conjugated fucoidan on PVA without affecting the surface roughness and topography of PVA. CDI can activate hydroxyl groups on PVA, forming imidazole active intermediates, which can further react with other nucleophiles [21a,28]. We have previously shown that the CDI reaction between polyvinyl alcohol hydrogels (PVA) and amine-containing molecules by XPS and Fourier-transform infrared spectroscopy [21a, 29]. Fucoidan contains hydroxyl groups, which are reactive to imidazole intermediates. We also synthesized aminated fucoidan to facilitate the conjugation with imidazole intermediates. The amount of EDA in the amination reaction of fucoidan was adjusted, and the results suggested that the reduction in amine groups on fucoidan did not necessarily decrease the probability of reaction between CDI-activated PVA (PVA-CDI) and aminated fucoidan (aF). But within the aF2-aF25 test groups, a higher concentration of amine groups contributed to better EC adhesion and lower thrombin generation.

The bioactivities of fucoidan have been reported to be affected by the structure, charge density, and conformation [8a,30]. We compared three fucoidan immobilization methods, PVA-SF, PVA-CDI-F, and PVA-CDI-aF. EC adhesion was substantially promoted by all fucoidan modifications compared to plain PVA, while the hemocompatibility showed drastic changes depending on the immobilization approach. We speculate that in the current experimental setting, cell adhesion may be less sensitive to the modification methods of fucoidan, compared to thrombogenicity. Fucoidan is known to have anticoagulant and antithrombotic activities, but the activities are dependent on multiple factors, such as concentration [31], molecular weight [32], and sulfate content [33]. In addition to anticoagulant activity, fucoidan has also been found to have a pro-coagulant activity when being used at a low concentration [34]. In our study, the fucoidan density on PVA-SF is one third of that on PVA-CDI-F and PVA-CDI-aF. This low fucoidan concentration on PVA-SF may have caused the fucoidan to express procoagulant activity, and thus induced significantly more thrombin generation in PRP *in vitro* and higher platelet and fibrin accumulation in whole blood *ex vivo*. PVA-CDI-F samples had comparable fucoidan concentration with PVA-CDI-aF; however, only PVA-CDI-aF exhibited low thrombogenicity. Comparing with native fucoidan, aminated derivative of fucoidan has been shown to be more potent in promoting clot lysis and thrombin inhibition [30]. Additionally, EDA was introduced to aminated-fucoidan, which may function as a spacer molecule and thus enable a more flexible conformation of fucoidan, which has been suggested to benefit the antithrombotic activity of fucoidan [35].

In the native environment, cytoskeletons are connected to ECM through FA complexes [36]. ECM proteins provide receptors of certain integrins that anchor cells to ECM. To explore the underlying

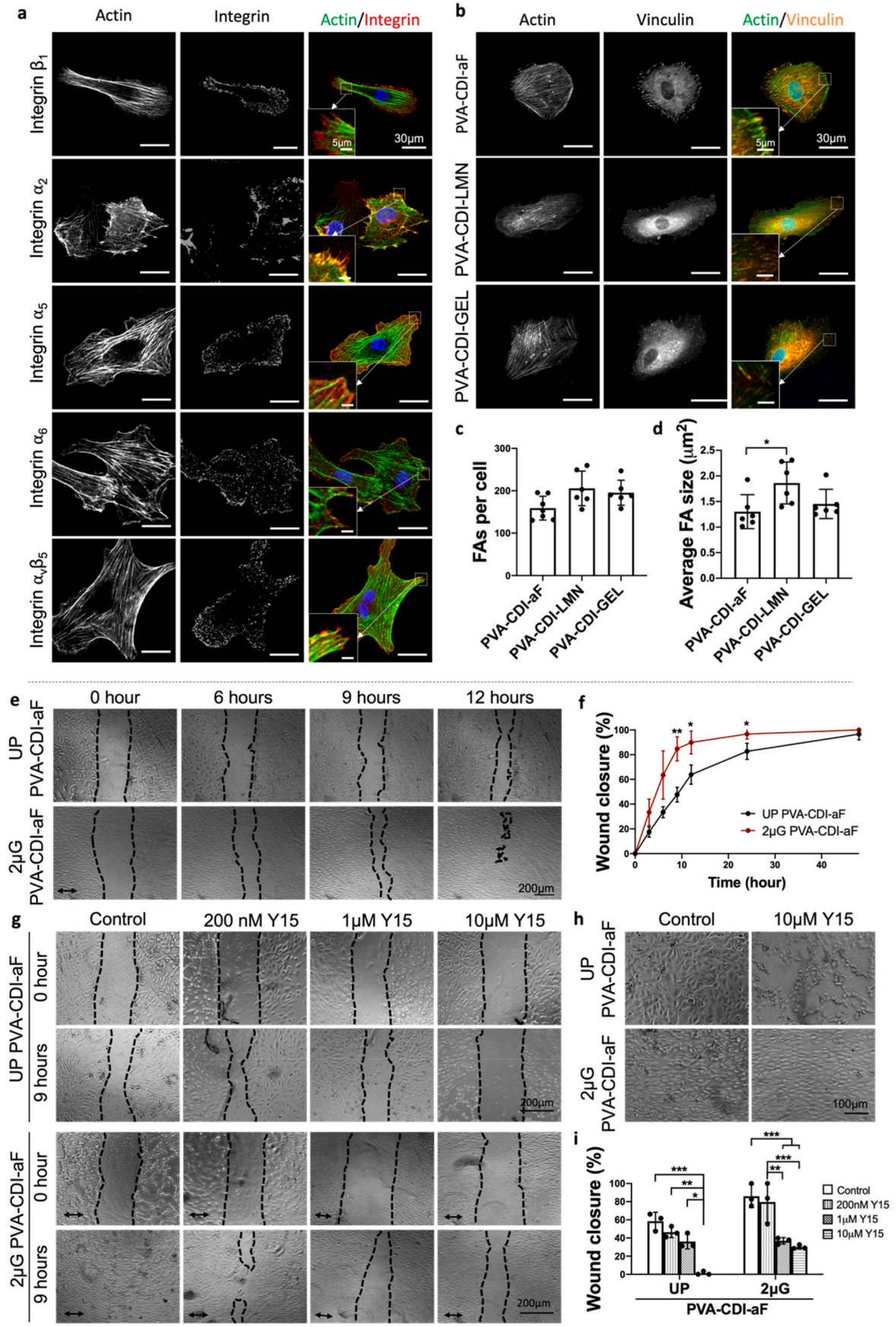

(caption on next page)

Fig. 4. Effect of focal adhesion signaling on endothelial cell adhesion and migration on PVA-CDI-aF. (**a**) Representative immunofluorescence staining image of integrin subunits β_1, α_2, α_5, α_6, and integrin $\alpha_v\beta_5$ formed by HUVECs on unpatterned PVA-CDI-aF imaged by confocal microscope. Scale bar = 30 μm. Blue denotes nuclei, green denotes actin, and red denotes integrins. Inset shows magnified view. Scale bar = 5 μm. (**b**) Representative images of immunofluorescence staining of vinculin, showing focal adhesions (FAs) formed by HUVECs on unpatterned PVA-CDI-aF, laminin-conjugated PVA (PVA-CDI-LMN) and gelatin-conjugated PVA (PVA-CDI-GEL) imaged by fluorescence microscope. Scale bar = 30 μm. Blue denotes nuclei, green denotes actin, and orange denotes vinculin. Inset shows magnified view. Scale bar = 5 μm. (**c**) Number of FAs per cell and (**d**) average FA size. n = 6, * indicates a significant difference using one-way ANOVA with $p < 0.05$. (**e**) Migration of HUVECs on unpatterned (UP) PVA-CDI-aF and 2 μm grating (2 μG) PVA-CDI-aF at 0 h, 6 h, 9 h, and 12 h in a wound healing assay. Scale bar = 200 μm. Arrow indicates the direction of 2 μm gratings. (**f**) Percentage of wound closure at different time points. n = 6, * and ** indicate a significant difference using one-way ANOVA with $p < 0.05$ and $p < 0.01$, respectively. (**g**) Effect of the focal adhesion kinase (FAK) inhibitor, Y15, at increasing concentrations on the migration of HUVECs. Scale bar = 200 μm. (**h**) Phase contrast images of HUVECs on UP and 2 μG PVA-CDI-aF in the absence (Control) and presence of 10 μM Y15. Scale bar = 100 μm. (**i**) Percentage of wound closure at 9 h with the addition of increasing concentration of Y15. n = 3, *, **, and *** indicate a significant difference using one-way ANOVA with $p < 0.05$, $p < 0.01$, and $p < 0.001$, respectively.

mechanism of fucoidan-facilitated EC adhesion, we examined the integrin and FA formation. We found that PVA-CDI-aF supported the formation of the integrin subunit β_1, α_2, α_5, α_6, and the integrin dimer $\alpha_v\beta_5$. The FA formation on fucoidan was similar to that on ECM proteins, gelatin and laminin (Fig. 4a and b). FAK is a central regulator of integrin-dependent cell adhesion [37]. The inhibition of FAK auto-phosphorylation using 10 μM Y15 significantly reduced HUVECs adhesion on PVA-CDI-aF (Fig. 4h), indicating the engagement of FAK signaling. Serum in cell culture media contains the cell adhesive protein fibronectin, which could be adsorbed to the substrate and promote cell adhesion [38]. We found that HUVECs were able to attach to PVA-CDI-aF in both serum containing endothelial growth media (EGM) and serum free media (SFM); however, removing serum from media significantly decreased cell spreading and pFAK formation. The supplement of 10 μg/ml fibronectin in SFM recovered the EC adhesion (Fig. 5a–d), suggesting that fibronectin participated in HUVEC adhesion to PVA-CDI-aF. To further demonstrate the involvement of fibronectin, we coated PVA-CDI-aF with fibronectin. Improved cell adhesion (Fig. 5g) and cell-cell junction protein expression (Fig. 5h) was observed on fibronectin-coated PVA-CDI-aF but not on fibronectin-coated PVA nor fibronectin-coated PVA-CDI. These results suggested that PVA-CDI-aF could recruit fibronectin on the material surface to encourage EC adhesion through FA signaling. Fibronectin is known to regulate EC spreading and migration through integrin $\alpha_5\beta_1$ [39]. HUVECs on PVA-CDI-aF expressed $\alpha_5\beta_1$, further suggesting the engagement of fibronectin in EC adhesion on PVA-CDI-aF. Fibronectin harbors heparin binding domains [40], and fucoidan has a similar structure as heparin. However, heparin has been shown to inhibit cell adhesion to fibronectin [41]. Using the CDI chemistry, we reacted PVA-CDI with 10 mg/ml heparin sodium solution or 1000 U/ml heparin drug solution. The conjugated heparin on PVA did not support HUVEC adhesion even with fibronectin in cell culture media (Supplementary Fig. 13). A previous study also reported that free fucoidan could bind to fibronectin through the heparin- and cell-binding domains, thus inhibiting adenocarcinoma cell adhesion to fibronectin [42]. Surprisingly, our studies showed that the conjugated aminated fucoidan on PVA-CDI-aF presents fibronectin to cells, improving EC adhesion. Thus, conjugated aminated is more beneficial to improve endothelial cell adhesion compared to free fucoidan and conjugated heparin. Further investigations will be required to reveal the binding mechanism.

In addition to biochemical cues, ECs are subjected to topographical cues provided by the EC basement membrane. Dimension and isotropy of substrate topography have been reported to markedly affect endothelial cell responses. Gratings with width of 1–10 μm have been shown to increase HUVEC adhesion and proliferation, while pillars with size of 1–10 μm reduced HUVEC proliferation [43]. Gratings that are narrower than cell size can induce EC alignment along the grating axis, which is beneficial for promoted directional migration. Conversely, gratings that are larger than cell size was reported to induce apoptosis and impair cell-cell contact [43,44]. In addition to the lateral dimension of the topography, cells are sensitive to the height or depth of substrate topography. Endothelial colony forming cells (ECFCs) cultured on pillars had decreased viability with increasing pillar height, and micro-pillars with height larger than 3 μm significantly decreased ECFC proliferation and spreading [45]. Alignment of ECs on grating structures was reported to increase with increasing depth of the gratings [46], and larger depth was reported to increase migration distance [47]. Grooves with depth larger than 1 μm significantly increased HUVEC spreading, and 1:1 aspect ratio (height: width) demonstrated the most potent effect [48]. In our previous studies, we compared the adhesion, proliferation, and functions of ECs on topography with different dimensions and isotropy [15,49]. Micro-sized gratings and pillars with 1:1 aspect ratio (height: width/diameter) and micro-sized lenses (Supplementary Table 2) exhibited the most significant difference on EC responses compared to unpatterned substrate, and thus were chosen for investigation in this study. In our previous study, topographical patterns on PVA could improve EC responses; however, without additional surface modification, ECs were not able to form monolayers [15a]. Using the aminated-fucoidan conjugation, we fabricated patterned PVA-CDI-aF that supported ECs forming a confluent functional EC layer. An endothelial layer that maintains its natural anticoagulant and anti-inflammatory activities is important to reduce intimal hyperplasia formation and maintain graft patency [50]. Nitric oxide (NO) released from ECs plays an important role in maintaining homeostasis [51], and previous studies have demonstrated that the NO production of ECs can be mediated by the substrate material [52]. We have previously reported that the endothelial nitric oxide synthase (eNOS) expression of HUVECs on fucoidan-modified PVA was significantly higher than that on glass coverslips, indicating that fucoidan does not affect the eNOS expression of HUVECs [13d]. Additionally, we previously found that concave and convex lenses significantly reduced the eNOS expression of human coronary artery endothelial cells compared to unpatterned surfaces, while gratings maintained a similar level of eNOS expression compared to unpatterned surface [49a]. The results suggested that grating may be more beneficial than lens for the NO production of ECs. ECs *in vivo* orients with the blood flow. In our study, ECs on gratings exhibited aligned morphology. Several studies have reported that aligned ECs have better anti-inflammatory and antithrombotic activities [53]. The alignment of ECs on gratings has demonstrated significantly higher prostacyclin (PGI2) and tissue plasminogen activator (tPA) [54], which are functional molecules that contribute to the anticoagulant activities of ECs. These findings further indicate that gratings could contribute to better antithrombotic activities of ECs.

In this study, we further characterized the anti-inflammatory properties of the formed EC monolayers on PVA-CDI-aF. Monocyte adhesion to EC monolayer and intravasation is a primary event in acute inflammation and subsequent generation of atherosclerosis [55]. Many studies suggested that a low level of monocyte adhesion to EC monolayer will be more beneficial for improved graft patency [56]. Conversely, some studies have reported that monocytes have the potential to transdifferentiate into ECs stimulated by vascular endothelial growth factor (VEGF) or monocyte chemoattractant protein-1 (MCP-1) [57]. However, the ability of monocytes to transdifferentiate into ECs without VEGF or MCP-1 stimulation was abolished [57a,58], and the monocytes differentiated into pro-inflammatory M1 phenotype macrophages. Thus, in this study, we selected 2 μG, which induced the lower monocyte

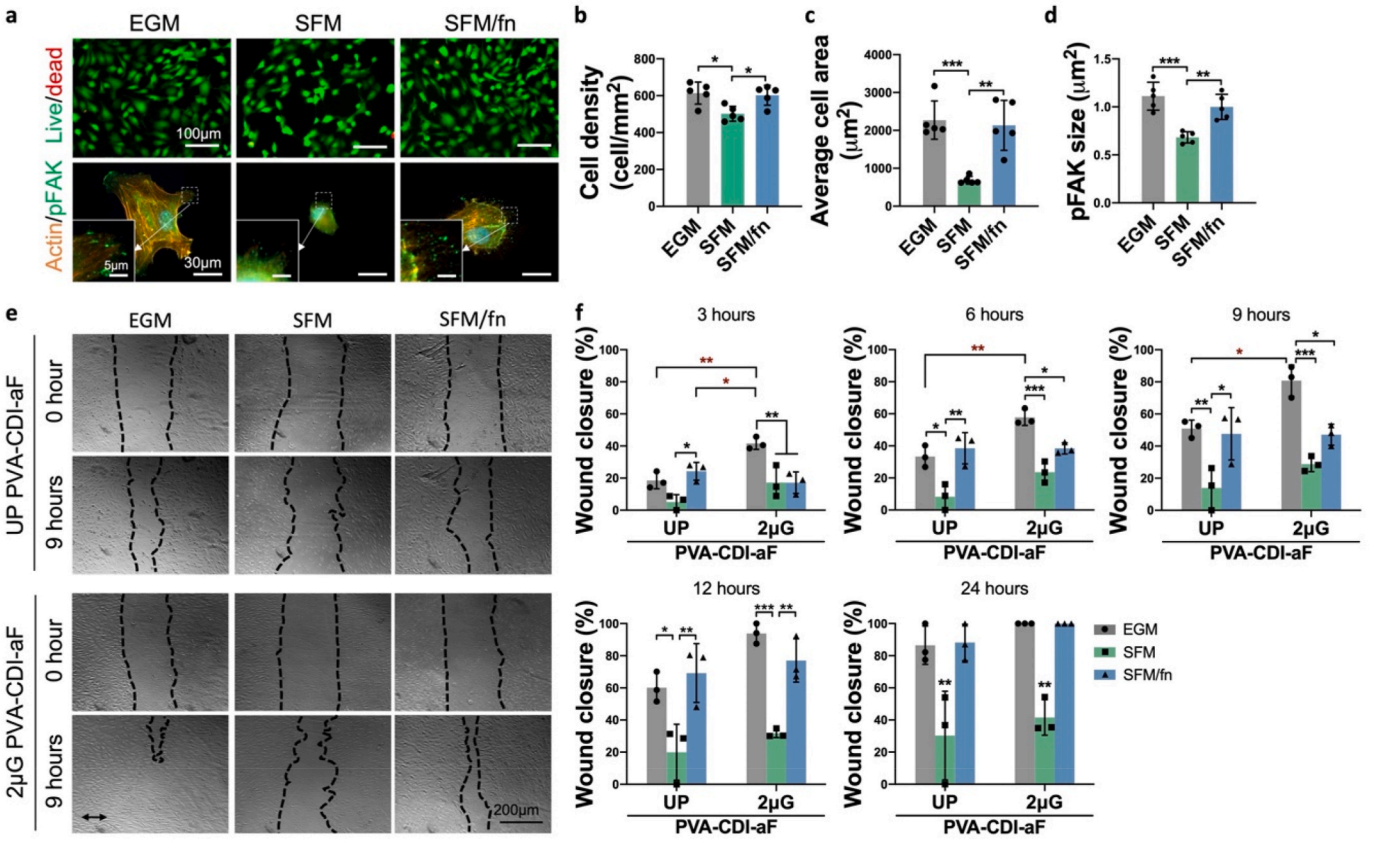

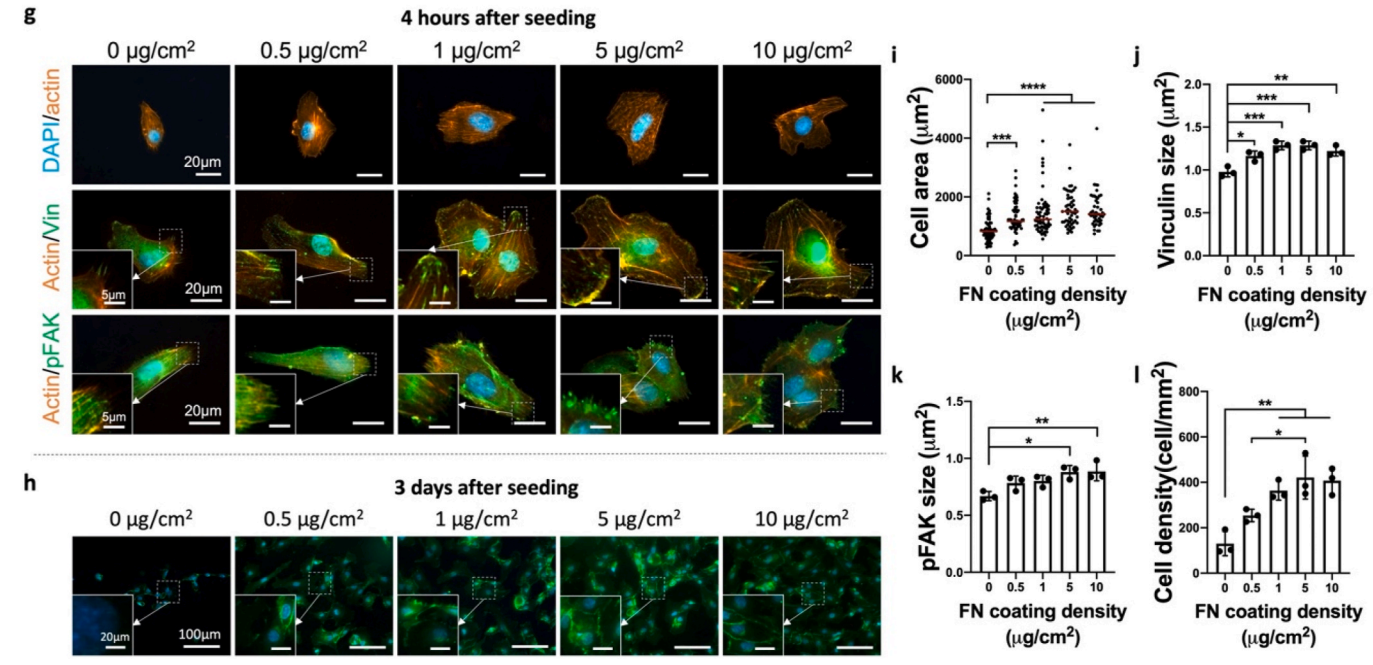

(caption on next page)

Fig. 5. Effect of fibronectin on endothelial cell adhesion and migration on PVA-CDI-aF. (**a**) Representative images of live/dead staining (top, scale bar = 100 μm) and pFAK staining (bottom, scale bar = 30 μm) of HUVECs on unpatterned PVA-CDI-aF in serum-containing media (EGM), serum free media (SFM), and fibronectin-supplemented SFM (SFM/fn). Inset shows magnified view. Scale bar = 5 μm. Quantification of (**b**) cell density, (**c**) average cell area, and (**d**) pFAK size. n = 6, *, **, and *** indicate a significant difference using one-way ANOVA with $p < 0.05$, $p < 0.01$, and $p < 0.001$, respectively. (**e**) Migration of HUVECs on unpatterned PVA-CDI-aF (UP) and 2 μm grating PVA-CDI-aF (2 μG) in different media. Scale bar = 200 μm. Arrow indicates the direction of the 2 μm gratings. (**f**) Percentage of wound closure at different time points. n = 3, *, **, and *** indicate a significant difference using one-way ANOVA with $p < 0.05$, $p < 0.01$, and $p < 0.001$, respectively. (**g**) Representative immunofluorescence staining images of F-actin staining (top, scale bar = 20 μm), vinculin staining (middle, scale bar = 30 μm), and pFAK staining (bottom, scale bar = 30 μm) of HUVECs on unpatterned PVA-CDI-aF coated with increasing concentrations of fibronectin at 4 h after cell seeding. Inset shows magnified view. Scale bar = 5 μm. (**h**) Representative images of VE-cadherin staining of HUVECs on unpatterned PVA-CDI-aF coated with increasing concentrations of fibronectin at 3 days after cell seeding. Scale bar = 100 μm. Blue denotes nuclei and green denotes VE-cadherin. Inset shows magnified view. Scale bar = 20 μm. Quantification of (**i**) cell area (60 cells from 3 samples were counted for each group), (**j**) average vinculin size (n = 3) and (**k**) average pFAK size (n = 3) at 4 h after cell seeding. *, **, ***, and **** indicate a significant difference using one-way ANOVA with $p < 0.05$, $p < 0.01$, $p < 0.001$ and $p < 0.0001$, respectively. (**l**) Quantification of cell density at 3 days after cell seeding. n = 3, * and ** indicate a significant difference using one-way ANOVA with $p < 0.05$ and $p < 0.01$, respectively.

adhesion to EC layers to proceed our studies. Additionally, ICAM-1 actively participate in the proinflammatory responses of ECs and increased expression of ICAM-1 has been shown to accelerate atherosclerotic lesion [59]. Among all topography, ECs on 2 μG had lowest ICAM-1 expression, further suggesting the benefit of 2 μG.

Topographies have also been shown to play a role in platelet adhesion, spreading, and activation [60]. The topographies on PVA-CDI-aF did not induce noticeable changes in platelet adhesion nor thrombin generation compared to plain PVA, which could be attributed to the unchanged surface energy and the antithrombotic activity of conjugated aF. Importantly, although PVA-CDI-aF could present fibronectin on the material surface, the thrombogenicity of PVA-CDI-aF was not elevated. Plasma fibronectin has been shown to be involved in hemostasis by integrating into fibrin [61]. Fucoidan have been reported to suppress fibrin polymerization [62] and promote fibrinolysis by stimulating plasminogen activation [63]. These findings together could explain the low thrombogenicity we have observed for PVA-CDI-aF samples.

Gratings can induce cell alignment and elongation and increase cell migration velocity and migration distance. In this study, we observed that HUVECs on 2 μG PVA-CDI-aF were aligned and had faster wound closure rate along the grating axis. Many studies have proposed that grating-driven cell alignment and migration is mediated by contact guidance. Contact guidance by gratings have been shown to induce lamellipodia constrained to grating direction [64]. Our previous study also demonstrated the microtubule organization centers were polarized induced by nano-gratings, which could promote directional migration from wound healing [16a]. Moreover, physical constraints of gratings can drive directional maturation and orientation of FAs [64]. Our previous study has found that FA formed by ECs on 2 μm gratings are elongated and oriented along grating axis [49a]. The constrained FA growth could induce the orientation of stress fibers, which provide anisotropic traction forces, consequently causing cell polarization, which serve as driving forces for directional cell migration [64]. In the current study, we found that by inhibiting FAK phosphorylation, HUVEC migration was significantly slowed and the effect of 2 μG on cell migration was abolished (Fig. 4i). Taken together, we speculate that 2 μG mediated FA signaling through contact guidance, induced EC alignment, and consequently accelerating HUVEC directional migration.

The common causes of graft failure in small diameter vascular graft are intimal hyperplasia and thrombus formation. Intimal hyperplasia (IH) formation could be driven by multiple factors, such as surgical trauma, lack of endothelialization, and mechanical properties mismatch. Many studies have correlated the anastomotic IH with mechanical injury and disturbed fluid dynamics, especially in the end-to-side anastomosis model [65]. The geometric discontinuity across the anastomoses between grafts and native blood vessels causes a blood flow disturbance or flow separation around the anastomoses, which causes endothelial injury followed by SMC and myofibroblasts proliferation [66]. Previous studies on ePTFE grafts have shown significant IH formation on the luminal surfaces of ePTFE [67]. We previously implanted 2 mm inner diameter ePTFE grafts in the same rabbit carotid artery endo-to-side implantation model as the current study [13d]. 2 out 3 ePTFE grafts were patent. IH formation was observed on the surface of ePTFE grafts and also on floor of the artery at the anastomoses. Interestingly, different from ePTFE grafts and other synthetic vascular grafts, the anastomotic IH in PVA and PVA-CDI-aF grafts was formed mainly on the floor of the native arteries. We speculate the mechanical properties, surgical injury and fluid dynamics may have been the main contributors of IH formation of PVA and PVA-CDI-aF grafts in the current end-to-side experimental setting. Using the same animal model as this study, we were able to significantly reduce the intimal hyperplasia formation on the floor of the artery by reducing the discrepancy of compliance between PVA grafts and artery [68]. Thus, we emphasize that both surface modification and optimal mechanical properties are crucial to mitigate intimal hyperplasia. PVA has been widely used in tissue engineering field. The tunable mechanical properties of PVA-STMP hydrogels are beneficial for vascular graft application. However, PVA is bioinert. Integration of PVA with surrounding tissue and unpredictable failure are concerning. Thus, in addition to luminal modification, functionalization of external surface is important to improve integration. We modified both luminal and external surfaces of PVA grafts using CDI-aF conjugation, cell adhesion on external surfaces was also observed. The cells did not appear to be ECs nor SMCs, due to the negative staining of VE-cadherin and α-SMA. Further characterization will be needed to determine the cell type. Additionally, delivery of bioactive molecules that mediate SMC or immune cell responses will be beneficial for long-term patency of PVA small diameter vascular grafts. The current study had only tested the *in vivo* patency for 4 weeks, studies that longer *in vivo* studies will be needed to determine long-term function and stability.

Different from *in vitro* cell culture conditions, in native environment, signals from both the extracellular matrix and the surrounding cells mediate EC responses. Previous studies have demonstrated that angiogenically stimulated monocytes or M2 macrophages support the formation of a functional confluent EC monolayer [69], while M1 macrophage inhibited EC functions [70]. Thus, in order to demonstrate the efficacy of 2 μG PVA-CDI-aF in enabling endothelialization in the actual *in vivo* condition, we characterized the tissue sections from plain PVA, UP PVA-CDI-aF, and 2 μG PVA-CDI-aF graft and compared the *in situ* endothelialization. We observed endothelialization on the lumen of UP PVA-CDI-aF, and 2 μG PVA-CDI-aF graft, proving the efficacy of the modification in promoting EC adhesion not only *in vitro* but also *in vivo*. The distance of human EC transanastomotic migration is severely limited to 1–2 cm only [5], even after prolonged implantation [71]. In acellular synthetic vascular grafts, fast endothelialization mainly occurs at the perianastomotic regions, and thus external stimulus to promote both EC adhesion and transanastomotic migration is required to endothelialize vascular grafts, especially in long grafts. In our previously published study, with the same animal model, ePTFE grafts failed to have any *in situ* endothelial cell adhesion [13d]. In the current studies, after 4 weeks of implantation, plain PVA grafts also lacked endothelial lining, thus generating significant blood clot at the anastomoses and

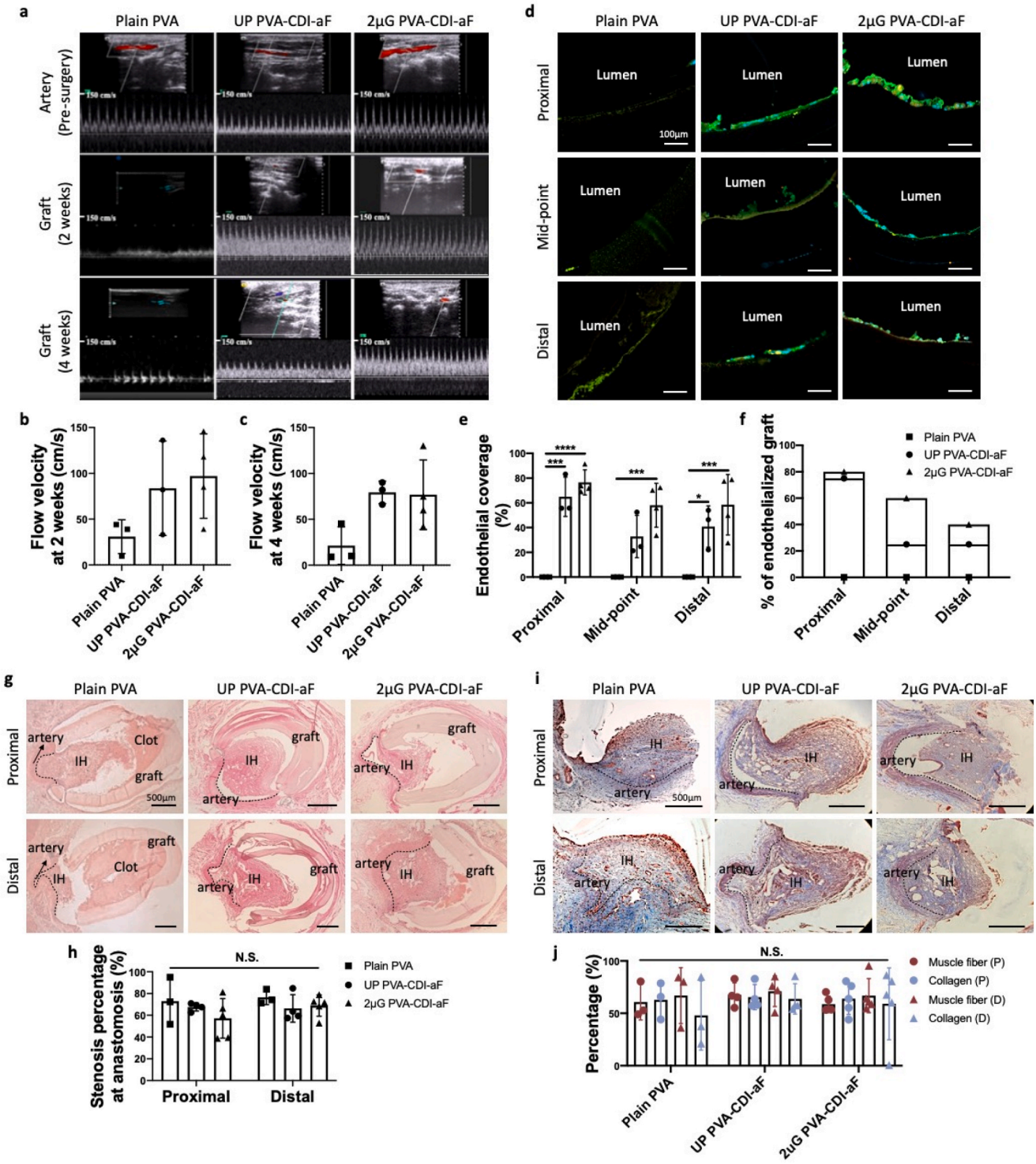

Fig. 6. *In vivo* performance of plain PVA, unpatterned (UP) PVA-CDI-aF, and luminal patterning with 2 μm gratings (2 μG) PVA-CDI-aF grafts in rabbit carotid artery end-to-side anastomosis model. (**a**) Representative ultrasound images of blood flow inside the grafts before surgery, 2 weeks after surgery and 4 weeks after surgery. Measurement of flow velocity inside the grafts at (**b**) 2 weeks and (**c**) 4 weeks. No statistical significance was observed. (**d**) Representative immunofluorescence staining images of endothelial cells in the lumen of implanted grafts. Graft segments that were close to the proximal end, at mid-point, and close to the distal end were imaged and analyzed. Scale bar = 100 μm. Blue denotes nuclei, green denotes VE-cadherin, and orange denotes CD31. (**e**) Endothelial coverage percentage of patent grafts. Occluded grafts were excluded from the analysis. n = 3 for plain PVA and UP PVA-CDI-aF, n = 4 for 2 μG PVA-CDI-aF. *, ***, and **** indicate a significant difference using two-way ANOVA with $p < 0.05$, $p < 0.001$, and $p < 0.0001$, respectively. (**f**) Percentage of endothelialized grafts (higher than 50% endothelial cell coverage) at each position. (**g**) Representative hematoxylin and eosin (H&E) staining images of proximal and distal anastomoses. Scale bar = 500 μm. IH indicates intimal hyperplasia. (**h**) Stenosis percentage at proximal and distal anastomoses. n = 4 for plain PVA and UP PVA-CDI-aF, n = 5 for 2 μG PVA-CDI-aF, no significance was observed. (**i**) Representative Masson's trichrome staining images of the stenosis in proximal and distal anastomoses of plain PVA, unpatterned PVA-CDI-aF, and 2 μG PVA-CDI-aF grafts. Scale bar = 500 μm. IH indicates intimal hyperplasia. Blue denotes collagen and red denotes muscle fibers. (**j**) Quantification of percentage of collagen and muscle fiber in the stenosis. P and D indicated the percentage at the proximal and distal anastomosis, respectively. n = 4 for plain PVA and UP PVA-CDI-aF, n = 5 for 2 μG PVA-CDI-aF. No statistical significance was observed.

inside the graft and leading to a 70% reduction in blood flow velocity compared to PVA-CDI-aF grafts detected at 14 days post-implantation. Conversely, UP PVA-CDI-aF grafts had endothelialization close to the anastomotic ends attributed from the enhancement function of immobilized fucoidan on EC adhesion, but the middle of grafts had low endothelial coverage due to limited migration of ECs. With the incorporation of 2 μm gratings, 2 μG PVA-CDI-aF grafts had endothelial coverage throughout the entire length of the grafts. Overall, the conjugated aF and 2 μm gratings combined to enable the *in situ* generation of endothelium on synthetic materials by stimulating the transanastomotic migration of endothelial cells.

4. Conclusions

In summary, we have successfully developed and tested a surface modification strategy using fucoidan and 2 μm gratings to improve *in situ* endothelialization of acellular off-the-shelf available synthetic vascular grafts without compromising hemocompatibility. We illustrated that fucoidan could attract fibronectin on the material surfaces, enabling integrin binding and FA formation and activating FAK signaling of ECs, thus promoting EC adhesion. The 2 μm gratings could provide contact guidance and further promoted FAK-mediated EC migration. The *in vivo* efficacy of this modification was evidenced by substantially increased luminal EC coverage and graft patency. The strategy can be further expanded to other synthetic materials to improve the long performance of blood-contacting devices.

5. Experimental section

Fabrication of PVA hydrogels. PVA hydrogels were fabricated by crosslinking PVA with sodium trimetaphosphate (STMP), as previously published [15a]. Briefly, 10% (w/v) PVA (average Mw 85,000–124,000, 87%–89% hydrolyzed, Sigma-Aldrich) aqueous solution was mixed with 15% (w/v) STMP solution and 30% (w/v) sodium hydroxide (NaOH) to generate a PVA crosslinking solution. Polydimethylsiloxane (PDMS; Sylgard 184, Dow Corning) with various topographies (as shown in Supplementary Table 2) was used as molds to prepare patterned PVA hydrogels. All PDMS molds were plasma-treated to increase surface energy. To prepare films, PVA crosslinking solution was cast on plain petri dishes or freshly plasma treated PDMS molds, followed by centrifugation. To prepare tubular grafts, a thin layer of patterned PDMS film was rolled around a cylindrical rod, followed by plasma treatment. The cylinder mold was then immersed and sonicated in PVA crosslinking solution for 1 h at 49 kHz. Afterwards, PVA crosslinking solution was dip-coated on the cylinder rod to form tubular grafts [20c]. PVA films and tubular grafts were kept in a cabinet with controlled temperature and humidity until fully crosslinked. Solutions of 10X phosphate buffer solution (PBS), 1X PBS, and deionized (DI) water were used to rehydrate and de-mold crosslinked PVA hydrogels. The grafts for implantation were curved in the middle by bending the cylindrical molds before de-molding procedures.

Amination of fucoidan. Amination of fucoidan using ethylenediamine (EDA, Sigma-Aldrich) was adopted from a previously published method [72]. Briefly, fucoidan (*Fucus vesiculosus*, Marinova) was aminated using ethylenediamine through carbonyldiimidazole (CDI, Sigma-Aldrich) reaction. Fucoidan (100 mg) was dissolved in 5 ml formamide, followed by the addition of 4 mg of CDI. After 1 h of stirring, different amount of EDA was added into the mixture and reacted under stirring overnight. The solution was then dialyzed in 3500 Da cut-off dialysis tubes against DI water for 5 days at room temperature and freeze dried.

Amine groups on the fucoidan was determined using fluorescamine, adopted from a previous protocol [72]. Briefly, 0.5 mg/ml aminated-fucoidan was dissolved in PBS. 1.5 ml of aminated-fucoidan solution was mixed with 0.5 ml of 3 mg/ml fluorescamine solution and incubated in darkness for 30 min. The fluorescence was measured at the excitation wavelength of 400 nm and the emission wavelength of 460 nm using a plate reader. EDA was used as a standard.

Modification of PVA hydrogels. PVA hydrogels were dried overnight at 60 °C to remove moisture. The hydrogels were then activated in 100 mg/ml CDI solution in dimethyl sulfoxide (DMSO) for 1 h at room temperature with 100 rpm shaking. The CDI-activated PVA hydrogels (PVA-CDI) were then wash 3 times in 1X PBS to remove excess CDI and incubated in 10 mg/ml aminated-fucoidan (PVA-CDI-aF) solution in PBS or 10 mg/ml native fucoidan (PVA-CDI-F) solution in PBS at 37 °C overnight. As a comparison, PVA hydrogels were directly soaked in 10 mg/ml native fucoidan solution at 37 °C overnight (PVA-SF). After overnight incubation, samples were washed 3 times with 1X PBS (Fig. 1a).

Gelatin conjugation on PVA was prepared by incubating PVA-CDI in 10 mg/ml gelatin type B (from bovine skin, Sigma-Aldrich) solution in PBS overnight at 37 °C (PVA-CDI-GEL). To prepare laminin-modified PVA, PVA-CDI was incubated in poly(L-lysine) overnight at 4 °C, followed by incubation in laminin (from mouse, Corning) solution for 1 h at 37 °C.

Quantification of fucoidan concentration. Concentration of fucoidan was determined by toluidine blue staining as previously described [13d]. Briefly, PVA hydrogels were cut into 1 cm^2 films and incubated in 500 μl of 50 μg/ml toluidine blue solution for 1 h with shaking. The absorbance of the supernatant at 631 nm was then measured to quantify the concentration of fucoidan. Fucoidan solution with a concentration ranging from 1.0 μg/ml-1.0 mg/ml was used for calibration.

Scanning electron microscope (SEM) measurement. SEM imaging was done with an environmental scanning electron microscope (FEI Quanta FEG 250 ESEM) in high vacuum mode at 20 kV. To prepare samples for imaging, PVA films was dried in a 60 °C oven overnight and mounted on aluminum stubs. No coating was applied prior to imaging.

X-ray photoelectron spectroscopy (XPS) measurement. X-ray photoelectron spectroscopy (XPS) was used to study the element composition on the surfaces of the samples. XPS survey spectra were measured in a Thermo-VG Scientific ESCALab 250 microprobe equipped with a monochromatic Al Kα source (1486.6 eV) at Waterloo Advanced Technology Laboratory (University of Waterloo, Waterloo, ON). The measurement was carried out under ultra-high vacuum (UHV) conditions with a pass energy of 50eV. The incidence angle of X-ray to sample was set at 45°, and the take-off angle was set at 90°. The atomic percentage of the samples was calculated in CasaXPS software.

Water contact angle measurement. Water contact angles of PVA and fucoidan-modified PVA films were measured using a captive bubble method with an optical contact angle system (OCA20, Future Digital Scientific Corp). PVA film samples were immersed in DI water, and an air bubble (4 μl) was injected into the water through a syringe. The bubble was allowed to attach to the surface of the samples and imaged by a camera. The contact angle was then calculated by the SCA20 software.

Mechanical property testing. Compliance of PVA grafts was determined by measuring the diameter change with changing pressures [20c]. PVA grafts were connected to a saline bag with adjustable height to change the internal pressure. The outer diameter of PVA grafts with internal pressure at 80 mmHg (D_{80}) and 120 mmHg (D_{120}) were measured and the compliance was calculated by: Compliance (%/40 mmHg) = $(D_{120}\text{-}D_{80})/D_{80} \times 100\%$. Burst pressure was determined by exposing the graft to increasing internal pressure induced by nitrogen gas until the graft burst. Uniaxial tensile testing was carried out using a Universal mechanical tester (UNMT-2MT, T1377, Center for Tribology, Inc.). PVA films were cut into rectangular strips and the dimensions were measured prior to testing. A gauge length of 1 cm, a stretch speed of 10 mm/min, and a loading cell of 100 kg were used.

In vitro hemocompatibility testing. *In vitro* hemocompatibility testing was done with rabbit platelet rich plasma (PRP), as previously described [13d]. Briefly, 9 ml of rabbit whole blood was primed with 1 ml of 3.8%

sodium citrate. Whole blood was centrifuged at 200 g for 10 min. PRP was collected after centrifugation and PVA samples were incubated with 200 μl PRP under shaking condition at 37 °C. After 1 h incubation, non-adherent PRP was collected for real-time thrombin generation assay (Technothrombin® Thrombin Generation Assay (TGA) kit, Diapharma) according to manufacturer's protocol. Three parameters, the starting time of thrombin generation (Lagtime), maximum thrombin generation rate (Peak), and total amount of generated thrombin (Total thrombin), were used to evaluate the thrombogenicity. Adhered platelets were either fixed with 2.5% glutaraldehyde for SEM imaging or lysed with 1% Triton X-100 for lactate dehydrogenase (LDH) analysis. Platelets for SEM imaging were dehydrated gradually using increasing concentration of ethanol. The LDH assay was done with an LDH kit (Roche) according to manufacturer's protocol.

Ex-vivo hemocompatibility testing. *Ex-vivo* hemocompatibility testing was done in an *ex-vivo* non-human primate shunt model as previously described [20a]. Samples were tested in two juvenile, male baboons (*papio anubus*, 10.4–11.4 kg). PVA vascular grafts with 4 mm inner diameter and 5 cm in length were incorporated in a chronic, arteriovenous shunt model with radiolabeled platelets and fibrin. Clinical ePTFE grafts (Gore) and collagen-coated (1 mg/mL equine collagen type I, Chrono-log Corp) ePTFE samples were used as clinical and positive controls, respectively. The grafts were subjected to whole blood flow at 100 ml/min for 1 h without administration of anticoagulant or antiplatelet therapies. The platelet accumulation, from autologous labelling with In^{111} was monitored every 1 min with a Brivo NM615 nuclear imaging camera (GE). Fibrin accumulation from homologous labelling with I^{125} was quantified by a 1480 Wizard gamma counter (PerkinElmer) after decay of the In^{111}. Graft patency was measured by imaging the graft samples using X-ray microcomputed tomography (microCT, Inveon, Siemens) and volume rendering software, Amira [29,73].

In vitro endothelial cell culture and seeding. Human umbilical vein endothelial cells (HUVECs, Lonza, pooled) were maintained in serum containing growth medium (EGM, Lifeline Cell Technology). The cells were cultured until 90% confluency before sub-culture. Confluent cells were washed once with HEPES buffered saline solution and detached by trypsinization. PVA films were UV-sterilized for 30 min, followed by incubation in antibiotic solution (10% penicillin-streptomycin and 1% amphotericin B) overnight at 4 °C. Prior to cell seeding, PVA films were washed thoroughly with PBS. To examine cell adhesion in culture media with different composition, cells were seeded in EGM, serum free media (SFM, ThermoFisher Scientific) or SFM supplemented with 10 μg/ml fibronectin (SFM/fn, concentration of fibronectin was according to the manufacturer's protocol, fibronectin was from bovine plasma, Sigma-Aldrich). The PVA samples were 1 cm^2 in area, and 500 μL of culture media was added into each sample to maintain cell growth. To evaluate cell adhesion on fibronectin-coated PVA-CDI-aF, PVA-CDI-aF films were coated with fibronectin solution for 1 h in an incubator before cell seeding. Images were taken using a Zeiss fluorescence microscope (Axio Observer Z1) and analyzed using ImageJ software.

Endothelial cell live/dead staining. HUVECs (P3-5) were seeded on PVA samples at a seeding density of 50,000 cells/cm^2 and cultured overnight to allow adhesion before live/dead staining. Live/dead staining was done according to supplier's protocol (ThermoFisher Scientific). Briefly, cells were washed once with 1x Dulbecco's phosphate-buffered saline (DPBS) and incubated with the mixture of calcein AM and ethidium homodimer-1 for 30 min. The cells were then washed once with 1x DPBS before imaging.

Endothelial cell monolayer formation. HUVECs (P3-5) were seeded on PVA samples at a seeding density of 50,000 cells/cm^2 and cultured for 2–3 days until confluent. Confluent cells were washed once with 1x DPBS, fixed with 4% paraformaldehyde (PFA), permeabilized with 0.1% Triton X-100, and blocked with 5% goat serum and 0.3% Triton X-100. Following blocking, the cells were stained with vascular endothelial cadherin (rabbit anti-VE-cad at 1:100, polyclonal, Cell Signaling Technology), platelet endothelial cell adhesion molecule (PECAM-1 or CD31, mouse-anti-PECAM-1 at 1:100, monoclonal, Abcam) and intercellular adhesion molecule-1 (ICAM-1, mouse-anti-ICAM-1 at 1:400, polyclonal, Abcam), and counterstained with DAPI to label nuclei. Images were taken using a Zeiss fluorescence microscope (Axio Observer Z1) and analyzed using ImageJ software. Cell circularity was measured in ImageJ based on the formula: circularity = 4pi(area/perimeter^2).

Monocyte adhesion to endothelium. HUVECs (P3-5) were seeded on unpatterned and patterned PVA films at 50,000 cells/cm^2 for 3 days until confluent. The endothelial cell layers were activated by incubation with 2.5 ng/ml tumor necrosis factor-α (TNF-α, Sigma-Aldrich) in culture media for 5 h. Human monocytes (U937, p13-14) were labeled with calcein-AM (Fisher scientific) and seeded on activated endothelial cells at 150,000 cells/cm^2. Samples were incubated for 45 min on a shaker, followed by staining with DAPI. Images were taken using Zeiss fluorescence microscope (Axio Observer Z1) and analyzed using ImageJ software.

Focal adhesion and integrin staining. Human umbilical vein endothelial cells (HUVECs) (P3-5) were seeded on plain PVA, unpatterned and patterned fucoidan-modified PVA films at 5000 cells/cm^2 for 12 h. The endothelial cells were then washed once with 1x DPBS, followed by fixation with 4% PFA, permeabilization with 0.1% Triton X-100, and blocking with 5% goat serum. The cells were then immunofluorescently-stained with vinculin (mouse-anti-vinculin at 1:400, Abcam), phosphorylated focal adhesion kinase (pFAK, rabbit-anti-vinculin at 1:200, Abcam) or integrin β1 (mouse-anti-integrin β1 at 1:50, DSHB), integrin α2 (mouse-anti-integrin α2 at 1:60, DSHB), integrin α5 (mouse-anti-integrin α5 at 1:50, DSHB), integrin α6 (mouse-anti-integrin α6 at 1:50, DSHB), and integrin αvβ5 (mouse-anti-integrin αvβ5 at 1:20, DSHB) with the corresponding fluorescently labeled secondary goat antibodies, and counter-stained with DAPI to label nuclei and phalloidin to label actin filaments. Images were taken using Zeiss 700 confocal microscope and Zeiss fluorescence microscope (Axio Observer Z1). To analyze the focal adhesions, images were enhanced using CLAHE algorithm in MATLAB, as previous described [74], followed by analysis using ImageJ to determine the size and density of focal adhesions.

Wound healing assay. Cell migration was studied with a wound healing assay. Briefly, HUVECs (P3-5) were seeded on unpatterned and 2 μm grating patterned fucoidan-modified PVA films. Cells were cultured in EGM for 3 days to allow cell monolayer formation. A wound was created by making a scratch on the cell monolayer with a triangular PDMS strip. On the 2 μm grating pattern, the wound was created perpendicular to the grating axis, to allow the cell migration direction to mimic *trans*-anastomotic migration in a vascular graft. After the scratch was made, detached cells were removed with DPBS. After DPBS washing, fresh media was added to the cells. The migration of the cells was tracked by taking images of the wounds using a Zeiss fluorescence microscope (Axio Observer Z1) equipped with a motorized stage at predetermined time points (0 h, 3 h, 6 h, 9 h, 12 h, 24 h, and 48 h). The area of the wound at different time points was measured with ImageJ. Percentage of wound closure was calculated by dividing the wound area at different time points to the wound area at 0 h. To determine cell migration in media with different composition, EGM was changed to SFM or SFM/fn after scratches were made. To evaluate the effect of focal adhesion kinase inhibitor on cell migration, Y15 was added into culture media after scratches were made.

Sterilization of PVA hydrogels. Sterilization with ethylene oxide (EtO) was done at Oregon National Primate Research Center (ONPRC) with the following procedure: preconditioning phase for 90 min at 55 °C and minimum relative humidity (RH) of 70% at puncture, EtO exposure phase for 60 min with EtO concentration of 759 mg/L at pressure range 400–650 mbar, and aeration phase for 12 h at 55 °C. Sterilization with gamma irradiation was done at the Southern Ontario Center for Atmospheric Aerosol Research in the University of Toronto. The irradiation was carried out with a Co-60 source (G.C. 220) at a dose of 25 kGy.

Implantation of PVA small diameter vascular graft. Implantation of PVA small diameter vascular grafts was done, as previously described [75]. Male New Zealand white rabbits (Charles River laboratories) with body weight of 3.5–4.0 kg were used in this study. The animals were anaesthetized using a continuous application of 400–800 ml/min oxygen and gas isoflurane (2–3%) through endotracheal intubation throughout the duration of the procedure. Anticoagulant (heparin, 200 IU/kg) was given intravenously prior to arterial clamping. Grafts were sterilized with EtO prior to implantation. Four unmodified PVA grafts, four unpatterned PVA-CDI-aF grafts, and five 2 μm grating PVA-CDI-aF grafts with inner diameter of 1.7 mm, length of 2 cm, and curvature of 1.4 cm radius in the middle were implanted on the right common carotid artery with end-to-side anastomoses, as shown in Supplementary Fig. 11. Ultrasound doppler imaging and measurements were done using Siemens Acuson X300 ultrasound system with a VF 8–3+ (8-3 MHz) linear transducer and imaging frequency of 10 MHz, post-surgery, at midpoints (2 weeks) and at endpoints (4 weeks) to detect blood flow and check graft patency.

Tissue processing and histological analysis. The standard practice to investigate stenosis and intimal hyperplasia requires pre-mortal pressurized perfusion. However, due to animal ethical protocol limitation, pre-mortal perfusion could not be performed. Heparin was administrated before euthanization and PFA was injected and pressurized as soon as the vascular graft was isolated. Explanted grafts were paraffin-embedded and sectioned. Hematoxylin and eosin (H&E) staining, immunofluorescence staining, and Masson's trichrome staining were done on the cross-sectional tissue slides from the anastomoses and the graft sections. Stenosis percentage was calculated by dividing the area of stenosis to the luminal area of the grafts from H&E-stained images using ImageJ. Endothelialization on the luminal surfaces was determined by immunofluorescence staining against VE-cadherin (rabbit anti-VE-Cad at 1:400, polyclonal, Cell Signaling Technology) and CD31 (mouse-anti-PECAM-1 at 1:400, monoclonal, Abcam). Tissue slides were permeabilized with 0.3% Triton-X and blocked with 5% goat serum, followed by incubating in primary antibody at 4 °C overnight and incubating in fluorescently labeled goat secondary antibody for 1 h at room temperature. Collagen and smooth muscle fiber percentage was determined by Masson's trichrome staining (Abcam). The RGB images from the Masson's trichrome staining were split into monochromatic images using the color deconvolution plugin in ImageJ. The blue and red channels were used for calculating the percentage of collagen and smooth muscle fibers, respectively. The percentage was calculated by dividing the area of collagen or smooth muscle fibers to the area of the intimal hyperplasia.

Statistical analysis. All statistical analysis was performed using GraphPad Prism 8. The values of all data were presented as mean ± Standard Deviation (SD). The number of biological replicas n varied among different experiments, and the n numbers were indicated in the legend of each figure. To determine statistical significance, *t*-test, one-way ANOVA with Tukey's post hoc test and two-way ANOVA with Sidak's post hoc test were used, as indicated in the figure legends. Statistical significance criterion was set at p value of <0.05.

Ethical statement

All rabbit studies were approved (#AUPP 16–09 and #AUPP 18–10) by the Animal Care Committee according to the Canadian Council on Animal Care's Guidelines, the requirements of Province of Ontario's Animals for Research Act, and the University of Waterloo's Guidelines for the Use of Animals in Research and Teaching. The shunt studies were approved by the Oregon National Primate Research Center (ONPRC) Institutional Animal Care and Use Committee. Baboons were cared for at ONPRC according to the "Guide to the Care and Use of Laboratory Animals'' prepared by the Committee on Care & Use of Laboratory Animals of the Institute of Laboratory Animal Resources, National Research Council (International Standard Book, Number 0-309-05377-3, 1996, the United States).

Data availability statement

The data that support the findings of this study are available from the corresponding author upon reasonable request.

CRediT authorship contribution statement

Yuan Yao: Conceptualization, Methodology, Validation, Formal analysis, Investigation, Writing – original draft, Writing – review & editing, Visualization. **Aung Moe Zaw:** Methodology, Investigation. **Deirdre E.J. Anderson:** Methodology, Investigation, Writing – review & editing. **YeJin Jeong:** Investigation, Writing – review & editing. **Joshua Kunihiro:** Investigation, Writing – review & editing. **Monica T. Hinds:** Writing – review & editing, Funding acquisition. **Evelyn K.F. Yim:** Conceptualization, Supervision, Writing – review & editing, Funding acquisition.

Declaration of competing interest

The authors declare that they have no known competing financial interests or personal relationships that could have appeared to influence the work reported in this paper.

Acknowledgements

This work was supported by the National Institutes of Health grants [NIH R01HL130274 and R01HL144113], NSERC-CREATE Training in Global Biomedical Technology Research and Innovation at the University of Waterloo [CREATE-509950-2018], Canada Foundation for Innovation (CFI35573), NSERC Research Tools and Instruments Fund (RTI-2018-00220), and the Oregon National Primate Research Center NIH grant award [P51OD011092]. We acknowledge Dr. Filip Konecny, Ms. Grace Pohan, Ms. Sabrina Mattiassi, Ms. Rebecca Mac, and the University of Waterloo Central Animal Facility for their help with the rabbit study. We thank Ms. Jennifer Johnson and the staff of the Oregon National Primate Research Center for the support of the baboon studies. We are grateful to Mr. Hanyue Shangguan for his technical assistance with the ultrasound imaging.

Appendix A. Supplementary data

Supplementary data to this article can be found online at https://doi.org/10.1016/j.bioactmat.2022.10.011.

References

[1] S. Jana, Acta Biomater. 99 (2019) 53.
[2] a) M. Carrabba, P. Madeddu, Front. Bioeng. Biotechnol. 6 (2018);
b) Y. Matsuzaki, K. John, T. Shoji, T. Shinoka, Appl. Sci. 9 (2019) 1274.
[3] F.O. Obiweluozor, G.A. Emechebe, D.-W. Kim, H.-J. Cho, C.H. Park, C.S. Kim, I. S. Jeong, Cardiovascular Engineering and Technology 11 (2020) 495.
[4] Y. Zhuang, C. Zhang, M. Cheng, J. Huang, Q. Liu, G. Yuan, K. Lin, H. Yu, Bioact. Mater. 6 (2021) 1791.
[5] P.F. Sánchez, E.M. Brey, J.C. Briceño, J Tissue Eng Regen Med 12 (2018) 2164.
[6] M. Wen, D. Zhi, L. Wang, C. Cui, Z. Huang, Y. Zhao, K. Wang, D. Kong, X. Yuan, ACS Appl. Mater. Interfaces 12 (2020) 6863.
[7] J. Kwon, Y. Koh, S.j. Yu, J.-H. Yoon, Thromb. Res. 163 (2018) 71.
[8] a) Y. Yao, E.K.F. Yim, Carbohydr. Polym. 270 (2021), 118347;
b) N.P. Patil, V. Le, A.D. Sligar, L. Mei, D. Chavarria, E.Y. Yang, A.B. Baker, Frontiers in Cardiovascular Medicine 5 (2018).
[9] a) Z. Wang, T. Liu, X. Chen, H. You, Q. Zhang, J. Xue, Y. Zheng, D. Luo, J. Ethnopharmacol. 210 (2018) 434;
b) M. Zhou, Y. Ding, L. Cai, Y. Wang, C. Lin, Z. Shi, Mol. Med. Rep. 17 (2018) 7089.
[10] Mourão, Mar. Drugs 13 (2015) 2770.
[11] J. Kim, I.-H. Bae, K. Lim, J. Park, D. Park, S.-Y. Lee, E.-J. Jang, M. Ji, D. Sim, Y. Hong, Y. Ahn, J. Park, J. Cho, J. Kang, I.-S. Kim, M. Jeong, Prog. Org. Coating 78 (2015) 348.
[12] A. Tariq, M. Athar, J. Ara, V. Sultana, S. Ehteshamul-Haque, M. Ahmad, Global Journal of Environmental Science and Management 1 (2015) 47.
[13] a) T.A. Kuznetsova, L.A. Ivanushko, E.V. Persiyanova, S.P. Ermakova, N. N. Besednova, Bull. Exp. Biol. Med. 166 (2019) 766;

b) N. Marinval, M. Morenc, M.N. Labour, A. Samotus, A. Mzyk, V. Ollivier, M. Maire, K. Jesse, K. Bassand, A. Niemiec-Cyganek, O. Haddad, M.P. Jacob, F. Chaubet, N. Charnaux, P. Wilczek, H. Hlawaty, Biomaterials 172 (2018) 14;
c) C. Ye Wang, H. Su, J. Wang, Y. Wang, H. Wang, A. Zhao, N. Huang, RSC Adv. 6 (2016), 56048;
d) Y. Yao, A.M. Zaw, D.E.J. Anderson, M.T. Hinds, E.K.F. Yim, Biomaterials 249 (2020), 120011.
[14] L. Cui, Y. Yao, E.K.F. Yim, APL Bioengineering 5 (2021), 031509.
[15] a) M.F. Cutiongco, S.H. Goh, R. Aid-Launais, C. Le Visage, H.Y. Low, E.K. Yim, Biomaterials 84 (2016) 184;
b) M. Kukumberg, Y. Yao, S.H. Goh, D.J.H. Neo, J.Y. Yao, E.K.F. Yim, Advanced Biosystems 2 (2018), 1700217.
[16] a) E.K.F. Yim, R.M. Reano, S.W. Pang, A.F. Yee, C.S. Chen, K.W. Leong, Biomaterials 26 (2005) 5405;
b) L. Ge, L. Yang, R. Bron, J.K. Burgess, P. van Rijn, ACS Appl. Bio Mater. 3 (2020) 2104;
c) A. Schwab, C. Hélary, R.G. Richards, M. Alini, D. Eglin, M. D'Este, Materials Today Bio 7 (2020), 100058.
[17] L. Wang, S.K. Murthy, G.A. Barabino, R.L. Carrier, Biomaterials 31 (2010) 7586.
[18] a) I. Firkowska-Boden, C. Helbing, T.J. Dauben, M. Pieper, K.D. Jandt, Langmuir 36 (2020), 11573;
b) D.K. Afflu, N.N. Nath, K. Gonzalez, L. Pocivavsek, N. Pitre, S. Velankar, E. Tzeng, J. Am. Coll. Surg. 231 (2020) S360.
[19] E.A. Kamoun, S.A. Loutfy, Y. Hussein, E.-R.S. Kenawy, Int. J. Biol. Macromol. 187 (2021) 755.
[20] a) M.F. Cutiongco, D.E. Anderson, M.T. Hinds, E.K. Yim, Acta Biomater. 25 (2015) 97;
b) M. Chaouat, C. Le Visage, W.E. Baille, B. Escoubet, F. Chaubet, M.A. Mateescu, D. Letourneur, Adv. Funct. Mater. 18 (2008) 2855;
c) Y. Jeong, Y. Yao, T.H. Mekonnen, E.K.F. Yim, Frontiers in Materials 7 (2021).
[21] a) M. Rizwan, Y. Yao, M.B. Gorbet, J.W. Tse, D.E.J. Anderson, M.T. Hinds, E.K. F. Yim, ACS Appl. Bio Mater. 3 (2020) 693;
b) G.T. Hermanson, in: G.T. Hermanson (Ed.), In Bioconjugate Techniques, third ed., Academic Press, Boston, 2013, p. 259, https://doi.org/10.1016/B978-0-12-382239-0.00004-2.
[22] J. Rayes, J.H. Bourne, A. Brill, S.P. Watson, Research and Practice in Thrombosis and Haemostasis 4 (2020) 23.
[23] a) D. Barros, I.F. Amaral, A.P. Pêgo, Biomacromolecules 21 (2020) 276;
b) A.M. Belkin, M.A. Stepp, Microsc. Res. Tech. 51 (2000) 280.
[24] A. Post, E. Wang, E. Cosgriff-Hernandez, Ann. Biomed. Eng. 47 (2019) 366.
[25] a) T. Grus, L. Lambert, M. Mlcek, H. Chlup, E. Honsova, M. Spacek, A. Burgetova, J. Lindner, BioMed Res. Int. 2018 (2018), 3519596;
b) D. Wang, X. Wang, X. Li, L. Jiang, Z. Chang, Q. Li, Mater. Sci. Eng. C 107 (2020), 110212;
c) A.J. Melchiorri, N. Hibino, J.P. Fisher, Tissue Eng. B Rev. 19 (2012) 292.
[26] M.F. Cutiongco, M. Kukumberg, J.L. Peneyra, M.S. Yeo, J.Y. Yao, A.J. Rufaihah, C. Le Visage, J.P. Ho, E.K. Yim, Front. Bioeng. Biotechnol. 4 (2016) 44.
[27] K. Ozaltin, M. Lehocky, P. Humpolicek, J. Pelkova, A. Di Martino, I. Karakurt, P. Saha, Polymers (2019) 11.
[28] J.M. Goddard, D. Erickson, Anal. Bioanal. Chem. 394 (2009) 469.
[29] N.M. Bates, H.E. Heidenreich, M.E. Fallon, Y. Yao, E.K.F. Yim, M.T. Hinds, D.E. J. Anderson, Front. Bioeng. Biotechnol. 8 (2020).
[30] M. Xing Wang, Q. Cao, A. Ji, H. Liang, S. Song, Mar. Drugs 17 (2019) 183.
[31] S. Zhang, S. Till, C. Knappe, J. Quinn, G. Catarello, J. Ray, F. Scheiflinger, C. M. Szabo, M. Dockal, Carbohydr. Polym. 115 (2015) 677.
[32] Z. Zhu, Q. Zhang, L. Chen, S. Ren, P. Xu, Y. Tang, D. Luo, Thromb. Res. 125 (2010) 419.
[33] G. Kopplin, A.M. Rokstad, H. Mélida, V. Bulone, G. Skjåk-Bræk, F.L. Aachmann, ACS Appl. Bio Mater. 1 (2018) 1880.
[34] M. Dockal, S. Till, S. Knappe, H.J. Ehrlich, F. Scheiflinger, Blood 118 (2011) 1208.
[35] Li, F. Lu, X. Wei, R. Zhao, Molecules 13 (2008) 1671.
[36] A. Zuidema, W. Wang, A. Sonnenberg, Bioessays 42 (2020), 2000119.
[37] P. Tapial Martínez, P. López Navajas, D. Lietha, Biomolecules 10 (2020) 179.
[38] M. Verdanova, P. Sauerova, U. Hempel, M.H. Kalbacova, Histochem. Cell Biol. 148 (2017) 273.
[39] Z. Al-Yafeai, A. Yurdagul, J.M. Peretik, M. Alfaidi, P.A. Murphy, A.W. Orr, Arterioscler. Thromb. Vasc. Biol. 38 (2018) 2601.
[40] X. Zhong, O. Arnolds, O. Krenczyk, J. Gajewski, S. Pütz, C. Herrmann, R. Stoll, Biochemistry 57 (2018) 6045.
[41] K. Lundmark, P.K. Tran, M. Kinsella, A. Clowes, T. Wight, U. Hedin, J. Cell. Physiol. 188 (2001) 67.
[42] J.M. Liu, J. Bignon, F. Haroun-Bouhedja, P. Bittoun, J. Vassy, S. Fermandjian, J. Wdzieczak-Bakala, C. Boisson-Vidal, Anticancer Res. 25 (2005) 2129.
[43] Y. Ding, Z. Yang, C.W.C. Bi, M. Yang, S.L. Xu, X. Lu, N. Huang, P. Huang, Y. Leng, ACS Appl. Mater. Interfaces 6 (2014), 12062.
[44] C.-C. Wu, Y.-S. Li, J.H. Haga, R. Kaunas, J.-J. Chiu, F.-C. Su, S. Usami, S. Chien, Proc. Natl. Acad. Sci. USA 104 (2007) 1254.
[45] L.E. Dickinson, D.R. Rand, J. Tsao, W. Eberle, S. Gerecht, J. Biomed. Mater. Res. 100A (2012) 1457.
[46] a) P. Uttayarat, G.K. Toworfe, F. Dietrich, P.I. Lelkes, R.J. Composto, J. Biomed. Mater. Res. 75A (2005) 668;
b) A. Sales, C. Picart, R. Kemkemer, Exp. Cell Res. 374 (2019) 1.
[47] C. Leclech, D. Gonzalez-Rodriguez, A. Villedieu, T. Lok, A.-M. Déplanche, A. I. Barakat, Nat. Commun. 13 (2022) 2797.
[48] D. Franco, M. Klingauf, M. Bednarzik, M. Cecchini, V. Kurtcuoglu, J. Gobrecht, D. Poulikakos, A. Ferrari, Soft Matter 7 (2011) 7313.
[49] a) S. Arora, S. Lin, C. Cheung, E.K.F. Yim, Y.-C. Toh, Biomaterials 234 (2020), 119747;
b) M.F.A. Cutiongco, B.M.X. Chua, D.J.H. Neo, M. Rizwan, E.K.F. Yim, Biomaterials 153 (2018) 70.
[50] A.O. Ward, M. Caputo, G.D. Angelini, S.J. George, M. Zakkar, Atherosclerosis 265 (2017) 266.
[51] V. Garcia, W.C. Sessa, Br. J. Pharmacol. 176 (2019) 189.
[52] D. Zou, J. Li, F. Kou, X. Luo, P. Yang, J. Mater. Sci. Technol. 91 (2021) 67.
[53] a) H. Jeon, J.H. Tsui, S.I. Jang, J.H. Lee, S. Park, K. Mun, Y.C. Boo, D.-H. Kim, ACS Appl. Mater. Interfaces 7 (2015) 4525;
b) F. Robotti, D. Franco, L. Bänninger, J. Wyler, C.T. Starck, V. Falk, D. Poulikakos, A. Ferrari, Biomaterials 35 (2014) 8479.
[54] J.-y. Chen, M. Hu, H. Zhang, B.-c. Li, H. Chang, K.-f. Ren, Y.-b. Wang, J. Ji, ACS Biomater. Sci. Eng. 4 (2018) 1976.
[55] M. Arakawa, T. Mita, K. Azuma, C. Ebato, H. Goto, T. Nomiyama, Y. Fujitani, T. Hirose, R. Kawamori, H. Watada, Diabetes 59 (2010) 1030.
[56] P. Theofilis, M. Sagris, E. Oikonomou, A.S. Antonopoulos, G. Siasos, C. Tsioufis, D. Tousoulis, Biomedicines 9 (2021) 781.
[57] a) S. Fujiyama, K. Amano, K. Uehira, M. Yoshida, Y. Nishiwaki, Y. Nozawa, D. Jin, S. Takai, M. Miyazaki, K. Egashira, T. Imada, T. Iwasaka, H. Matsubara, Circ. Res. 93 (2003) 980;
b) R.J. Smith, B. Nasiri, J. Kann, D. Yergeau, J.E. Bard, D.D. Swartz, S. T. Andreadis, Nat. Commun. 11 (2020) 1622.
[58] R.J. Smith Jr., T. Yi, B. Nasiri, C.K. Breuer, S.T. Andreadis, Faseb. J. 33 (2019) 5089.
[59] C.-C. Chang, C.-F. Chu, C.-N. Wang, H.-T. Wu, K.-W. Bi, J.-H.S. Pang, S.-T. Huang, Phytomedicine 21 (2014) 207.
[60] L.B. Koh, I. Rodriguez, S.S. Venkatraman, Biomaterials 31 (2010) 1533.
[61] Y. Wang, A. Reheman, C.M. Spring, J. Kalantari, A.H. Marshall, A.S. Wolberg, P. L. Gross, J.I. Weitz, M.L. Rand, D.F. Mosher, J. Freedman, H. Ni, J. Clin. Invest. 124 (2014) 4281.
[62] J. Wang, Q. Zhang, Z. Zhang, H. Song, P. Li, Int. J. Biol. Macromol. 46 (2010) 6.
[63] R. Ghebouli, S. Loyau, M. Maire, P. Saboural, J.P. Collet, M. Jandrot-Perrus, D. Letourneur, F. Chaubet, J.B. Michel, Thromb. Haemostasis 118 (2018) 42.
[64] A. Ray, O. Lee, Z. Win, R.M. Edwards, P.W. Alford, D.-H. Kim, P.P. Provenzano, Nat. Commun. 8 (2017), 14923.
[65] Y. Jeong, Y. Yao, E.K.F. Yim, Biomater. Sci. 8 (2020) 4383.
[66] a) K. Sakai LuodingZhu, Phys. Fluids 33 (2021), 051905;
b) A. Post, P. Diaz-Rodriguez, B. Balouch, S. Paulsen, S. Wu, J. Miller, M. Hahn, E. Cosgriff-Hernandez, Acta Biomater. 89 (2019) 84;
c) V.S. Sottiurai, S. Lim Sue, E.L. Feinberg, , II, W.L. Bringaze, A.T. Tran, R. C. Batson, Eur. J. Vasc. Surg. 2 (1988) 245;
d) V.S. Sottiurai, J.S.T. Yao, R.C. Batson, S.L. Sue, R. Jones, Y.A. Nakamura, Ann. Vasc. Surg. 3 (1989) 26.
[67] a) P.H. Lin, C. Chen, R.L. Bush, Q. Yao, A.B. Lumsden, S.R. Hanson, J. Vasc. Surg. 39 (2004) 1322;
b) T. Masaki, R. Rathi, G. Zentner, J.K. Leypoldt, S.F. Mohammad, G.L. Burns, L. Li, S. Zhuplatov, T. Chirananthavat, S.-J. Kim, S. Kern, J. Holman, S.W. Kim, A. K. Cheung, Kidney Int. 66 (2004) 2061.
[68] Y. Yao, G. Pohan, M.F.A. Cutiongco, Y. Jeong, J. Kunihiro, A.M. Zaw, H. Shnagguang, A.C.H. Yu, E.K.F. Yim, Biomaterials Science, BM, 2022.
[69] a) A. Mayer, T. Roch, K. Kratz, A. Lendlein, F. Jung, Acta Biomater. 8 (2012) 4253;
b) Y.-c. Hou, F. Witte, J. Li, S. Guan, Smart Materials in Medicine 3 (2022) 188.
[70] a) N. Jetten, S. Verbruggen, M.J. Gijbels, M.J. Post, M.P.J. De Winther, M.M.P. C. Donners, Angiogenesis 17 (2014) 109;
b) K.Q. Wu, C.S. Muratore, E.-Y. So, C. Sun, P.M. Dubielecka, A.M. Reginato, O. D. Liang, Am. J. Pathol. 187 (2017) 2102.
[71] a) T. Pennel, P. Zilla, D. Bezuidenhout, J. Vasc. Surg. 58 (2013) 1053;
b) D.E. Heath, Macromol. Chem. Phys. 218 (2017), 1600574.
[72] A.N. Lukyanov, R.M. Sawant, W.C. Hartner, V.P. Torchilin, J. Biomater. Sci. Polym. Ed. 15 (2004) 621.
[73] A. Gupta, C.M. Johnston, M.T. Hinds, D.E.J. Anderson, Methods and Protocols 3 (2020).
[74] R. Muhammad, S.H. Lim, S.H. Goh, J.B.K. Law, M.S.M. Saifullah, G.W. Ho, E.K. F. Yim, Biomater. Sci. 2 (2014) 1740.
[75] Y. Yao, Y. Jeong, A.M. Zaw, M. Kukumberg, E.K.F. Yim, in: F. Zhao, K.W. Leong (Eds.), In Vascular Tissue Engineering: Methods and Protocols, Springer US, New York, NY, 2022, p. 177, https://doi.org/10.1007/978-1-0716-1708-3_15.